NAVAL POSTGRADUATE SCHOOL

MONTEREY, CALIFORNIA

THESIS

A NUMERICAL STUDY OF THE VALIDITY REGIMES OF WEAK FLUCTUATION THEORY FOR OCEAN ACOUSTIC PROPAGATION THROUGH RANDOM INTERNAL WAVE SOUND SPEED FIELDS

by

Serdar Tombul

March 2007

Thesis Advisor: John Colosi
Second Reader: Roberto Cristi

Approved for public release; distribution is unlimited

THIS PAGE INTENTIONALLY LEFT BLANK

REPORT DOCUMENTATION PAGE			Form Approved OMB No. 0704-0188

1. AGENCY USE ONLY *(Leave blank)*	2. REPORT DATE March 2007	3. REPORT TYPE AND DATES COVERED Master's Thesis

4. TITLE AND SUBTITLE A Numerical Study of the Regimes of Validity of Weak Fluctuation Theory for Ocean Acoustic Propagation through Random Internal Wave Sound Speed Fields	5. FUNDING NUMBERS
6. AUTHOR(S) Serdar Tombul	
7. PERFORMING ORGANIZATION NAME AND ADDRESS Naval Postgraduate School Monterey, CA 93943-5000	8. PERFORMING ORGANIZATION REPORT NUMBER
9. SPONSORING /MONITORING AGENCY NAME(S) AND ADDRESS(ES) N/A	10. SPONSORING/MONITORING AGENCY REPORT NUMBER

11. SUPPLEMENTARY NOTES The views expressed in this thesis are those of the author and do not reflect the official policy or position of the Department of Defense or the U.S. Government.

12a. DISTRIBUTION / AVAILABILITY STATEMENT Approved for public release; distribution is unlimited	12b. DISTRIBUTION CODE

13. ABSTRACT

Results of the ATOC project's AET experiment have shown that at 75 Hz Rytov theory may be used for predicting the phase variations. This paper is focused on establishing the regimes of validity for Rytov theory at 75-400 Hz acoustic frequency range and up to 200 km distance. Ray paths correspond to grazing angles of 0°,5°,10° and 14° are considered, thus spanning the range of possible ray geometry from surface reflection to axial propagation. We find that the Rytov and simulation spectra are in very good agreement in the frequency range from the buoyancy frequency up to a grazing angle dependent on the transition frequency between 1 and 0.2 cph. For frequencies less than the transition frequency the Rytov spectra are in fairly good agreement with the simulations for all ranges and grazing angles between 0º and 10º. For the 14º beam the Rytov theory dramatically under predicts the spectral energy at frequencies less than 1 cph. When there is significant variability in phase and log-amplitude, we also find that significant spectral energy can exist at frequencies greater than the buoyancy frequency. This energy is not predicted by the Rytov model and represents the effect of strong interference and scattering not treated in the weak fluctuation approach of the Rytov theory. This study will increase the interest in the weak fluctuation theory (WFT) as an acoustic prediction tool.

14. SUBJECT TERMS Underwater Acoustics, Signal Processing, Oceanography, Rytov Theory, Internal Waves, Parabolic Equation, Garrett-Munk Spectrum, Phase, Log-Amplitude	15. NUMBER OF PAGES 103
	16. PRICE CODE

17. SECURITY CLASSIFICATION OF REPORT	18. SECURITY CLASSIFICATION OF THIS PAGE	19. SECURITY CLASSIFICATION OF ABSTRACT	20. LIMITATION OF ABSTRACT
Unclassified	Unclassified	Unclassified	UL

NSN 7540-01-280-5500 Standard Form 298 (Rev. 2-89)
Prescribed by ANSI Std. 239-18

THIS PAGE INTENTIONALLY LEFT BLANK

Approved for public release; distribution is unlimited

A NUMERICAL STUDY OF THE REGIMES OF VALIDITY OF WEAK FLUCTUATION THEORY FOR OCEAN ACOUSTIC PROPAGATION THROUGH RANDOM INTERNAL WAVE SOUND SPEED FIELDS

Serdar Tombul
Lieutenant Junior Grade, Turkish Navy
B.S., Turkish Naval Academy, 2001

Submitted in partial fulfillment of the
requirements for the degree of

MASTER OF SCIENCE IN ENGINEERING ACOUSTICS
AND
MASTER OF SCIENCE IN ELECTRICAL ENGINEERING

from the

NAVAL POSTGRADUATE SCHOOL
March 2007

Author: Serdar Tombul

Approved by: John Colosi
Thesis Advisor

Roberto Cristi
Second Reader

Kevin B. Smith
Chair, Engineering Acoustics Academic Committee

Jeffrey Knorr
Chairman, Department of Electrical and Computer Engineering

THIS PAGE INTENTIONALLY LEFT BLANK

ABSTRACT

Results of the Acoustic Thermometry of Ocean Climate (ATOC) project's experiments have shown that at 75 Hz, the Rytov acoustic scattering theory using the Garrett-Munk (GM) internal wave spectrum may be used for predicting the variations of log-amplitude and phase. Using Monte Carlo methods, this paper is focused on establishing the regimes of validity of the Rytov theory within the 75–400 Hz acoustic frequency range and for propagation ranges up to 200 km. Ray paths corresponding to grazing angles of 0°, 5°, 10° and 14° are considered, thus spanning the range of possible ray geometry from surface reflection to axial propagation. Investigations show that the Rytov and simulation spectra are in very good agreement in the frequency range from the buoyancy frequency up to a grazing-angle-dependent transition frequency between 1 and 0.2 cph. For frequencies less than the transition frequency, the Rytov spectra are in fairly good agreement with the simulations for all ranges and grazing angles between 0º and 10º. For the 14º beam, the Rytov theory dramatically underpredicts the spectral energy at frequencies less than 1 cph. When there is strong variability in phase and log-amplitude, analysis shows significant spectral energy can exist at frequencies greater than the buoyancy frequency. This energy is not predicted by the Rytov model and represents the effect of strong interference and scattering not treated in the weak fluctuation approach of the Rytov theory. This study increases the relevance of the weak fluctuation theory (WFT) as an acoustic prediction tool.

THIS PAGE INTENTIONALLY LEFT BLANK

TABLE OF CONTENTS

LIST OF FIGURES

LIST OF TABLES

THIS PAGE INTENTIONALLY LEFT BLANK

ACKNOWLEDGMENTS

There are many people in my life who have the right to be proud of any success that I have. First of all, I would like to thank my family, who has helped me through every stage of my life. I will never forget any of my teachers who have thought me at least one word. Special thanks to my academic advisor and teacher Daphne Kapolka for helping me through all the steps that I needed to have a dual degree at Naval Postgraduate School.

I am very lucky to have very special thesis advisors as John Colosi and Roberto Cristi. I am proud to be your student and so happy to learn from your experience and knowledge. It is very hard to express my gratitude to John Colosi after all the time he shared with me to make this thesis better and useful for further studies. Thank you for everything. I would like to thank both of you as being so gentle and helpful.

I am grateful to my wife to be the source of my happiness in life. I owe you many thanks for your support and patience. You are my beautiful princess. I will love you forever.

THIS PAGE INTENTIONALLY LEFT BLANK

EXECUTIVE SUMMARY

The objective of this thesis is to examine efficient reduced physical models for estimating acoustic propagation through the fluctuating ocean. This research is a study to predict acoustic propagation statistics using "simple" analytical models rather than doing intensive and time-consuming Monte Carlo computations.

The theory of wave propagation through random media was pioneered by Soviet workers in the 1950s and 1960s in an effort to understand optical propagation through the atmosphere. Using the important results of Kolmogorov's homogenous isotropic turbulence model, a perturbation approach developed by Rytov was applied successfully in many experiments in which the optical fluctuations were weak. Inspired by these results, ocean acousticians spent many unsuccessful years trying to apply the homogenous isotropic theory to the ocean. In the 1970s oceanographers finally started talking with ocean acousticians, and it was discovered that internal gravity waves in the ocean are the primary cause of random sound speed fluctuations: internal waves are neither homogenous nor isotropic. Furthermore, internal waves have their own intrinsic wave-like time dependence, existing between the local buoyancy and Coriolis frequencies. In addition, in the ocean sound travels along curved ray paths rather than straight-line paths. With the advent of the Garret-Munk (GM) internal wave spectrum and the adaptation of the Rytov method to the ocean by Munk and Zachariasen, the prediction of ocean acoustic fluctuations were on a much firmer footing.

The MATE experiment using frequencies of 2–13 kHz showed that the Rytov theory can accurately predict the frequency spectrum of phase variations, but it also showed that the Rytov theory was not working for the frequency spectrum of intensity fluctuations. In a later experiment as part of the Acoustic Thermometry of Ocean Climate (ATOC) project's Acoustic Engineering Test (AET), 75 Hz signals were transmitted to a range of 87 km with a bandwidth of 30 Hz. Colosi and Xu (2007) examined the acoustic variability in the AET experiment. Assuming the ocean sound speed fluctuation spectrum had the GM (Garrett-Munk) form, they computed the intensity spectrum using the Rytov theory of Munk and Zachariasen (1976), and found that the theory matched the

observations fairly well. Following this success, this thesis will investigate the limits of applicability of the Rytov theory for low acoustic frequencies and a variety of ray geometries. This research addresses the important problem of characterizing the acoustic uncertainty in the ocean sound channel.

Rytov theory for random ocean media describes the mechanism of weak, multiple forward scattering. In this regime, phase fluctuations lead to intensity fluctuations. Phase fronts are distorted, leading to focusing and defocusing. The Rytov theory describes an important resonance condition in which only internal waves whose crests are aligned with the sloping ray path will contribute to the scattering. The alignment of the crests means that only internal waves whose wave numbers are perpendicular to the acoustic ray will contribute to the scattering. This theory therefore treats all of the complications in ocean acoustic propagation through internal waves, namely ray paths whose angle changes gradually with range, and inhomogeneous and anisotropic internal-wave-induced sound speed perturbations.

This thesis uses the acoustic observable of the frequency spectrum of phase and log-amplitude for the analysis, since many other acoustic observables, namely amplitude and phase correlation functions and coherence, can be derived from these spectra directly. Using Monte Carlo parabolic equation numerical simulation methods with random realizations of GM internal waves, this study established the acoustic propagation range and acoustic frequency limitations of the theory, as a function of ray path geometry. Monte Carlo methods are accurate but very time consuming; the Rytov theory, on the other hand, has a regime where it is very accurate and computationally efficient. The Monte Carlo numerical simulations were carried out at acoustic frequencies of 75, 200, and 400 Hz, and for the range evolutions of four acoustic ray paths up to a maximum range of 200 km. Ray paths correspond to grazing angles of 0°, 5°, 10° and 14°, thus spanning the range of possible ray geometry from surface reflection to axial propagation. At a series of different ranges from the source, frequency spectra have been computed and compared to the theory to establish regimes of validity and the mechanism by which the theory breaks down.

For all acoustic frequencies and beam grazing angles, results show that the Rytov and simulation spectra are in very good agreement in the frequency range from the buoyancy frequency up to a grazing-angle-dependent transition frequency between 1 and 0.2 cph. In this frequency range the slope of the spectra is nearly -3. However, the spectra of log-amplitude at the longer ranges and higher acoustic frequencies show some weakening of the -3 slope. The Rytov resonance with perpendicular wave numbers limits the influence of low-frequency internal waves for the frequencies less than the transition frequency. The Rytov theory spectra are in fairly good agreement with the simulations for all ranges and grazing angles between 0º and 10º. For the 14º beam, in which there is significant surface interaction, the Rytov theory dramatically underpredicts the spectral energy at frequencies less than 1 cph, demonstrating a breakdown in the Rytov resonance condition. When there is strong variability in phase and log-amplitude, we also find that significant spectral energy can exist at frequencies greater than the buoyancy frequency (the maximum internal wave frequency). This energy is not predicted by the Rytov model and represents the effect of strong interference and scattering not treated in the weak fluctuation approach.

These results help to establish the regimes of validity of the Rytov theory at low frequencies, and show that in these regions there is an efficient method for predicting the space-time scales of acoustic phase and intensity fluctuations. These results need to be further validated with ocean experiments so that better sonar system algorithms can be established.

THIS PAGE INTENTIONALLY LEFT BLANK

I. INTRODUCTION

Ocean acoustics is a rather simple topic in principle: if one specifies the space-time structure of the ocean sound speed field, one can in principle compute, using the wave equation, the acoustic pressure field for any arrangement of sources and receivers. However in practice, ocean acousticians have rather incomplete information about the space-time structure of the ocean sound speed field. Furthermore, the ocean has many dynamic and complex fluid motions that can only be treated stochastically and not deterministically. Thus ocean acoustic propagation is in essence statistical in nature, as has been revealed by decades of experiments since the 1960's (Flatte et al., 1979; Munk et al., 1996). Characterization of the statistics of ocean acoustic signals is therefore an important prerequisite to the design of useful systems for ocean remote sensing, communication, and navigation.

The primary motivation of this thesis is to find regimes of acoustic frequency, propagation range, and acoustic ray path geometry where computationally efficient reduced physics models of sound transmission through the fluctuating ocean can be accurately applied to estimate the space-time scales of acoustic variability.

A. SOUND TRANSMISSION THROUGH A FLUCTUATING OCEAN

Sound transmission through a fluctuating ocean is an active area of research that has matured with the studies of Stanley M. Flatte (1975), Roger Dashen (1979), Walter H. Munk (1976), Kenneth M. Watson (1979), Fredrik Zachariasen (1976), B.J. Uscinski, T.E. Ewart (1998), John A. Colosi (2007), and many other researchers from all over the world.

An understanding of acoustic fluctuations and variability is important because these effects impose the ultimate limits on acoustical remote sensing.

The theory of wave propagation through random media was pioneered by Soviet workers in the 1950s and 1960s in an effort to understand optical propagation through the atmosphere. Using the important results of Kolmogorov's homogenous isotropic turbulence model, a perturbation approach developed by Rytov was applied successfully

in many experiments in which the optical fluctuations were weak. Inspired by these results, ocean acousticians spent many unsuccessful years trying to apply the homogenous isotropic theory to the ocean. In the 1970s oceanographers finally started talking with ocean acousticians, and it was discovered that internal gravity waves in the ocean are the primary cause of random sound speed fluctuations: internal waves are neither homogenous nor isotropic. Furthermore, internal waves have their own intrinsic wave-like time dependence, existing between the local buoyancy and Coriolis frequencies. In addition, in the ocean sound travels along curved ray paths, rather than straight-line paths. With the advent of the Garret-Munk (GM) internal wave spectrum and the adaptation of the Rytov method to the ocean by Munk and Zachariasen, the prediction of ocean acoustic fluctuations were on a much firmer footing.

The Rytov theory describes an important resonance condition in which only internal waves whose crests are aligned with the sloping ray path will contribute to the scattering. The alignment of the crests means that only internal waves whose wave numbers are perpendicular to the acoustic ray will contribute to the scattering. This theory therefore treats all of the complications in ocean acoustic propagation through internal waves, namely ray paths whose angle changes gradually with range, and inhomogeneous and anisotropic internal-wave-induced sound speed perturbations.

During the last decade researchers have used computer modeling and simulation as a tool to analyze and compare the theories as well as to validate them with ocean experiments. These efforts have developed better theories to estimate many ocean acoustic observables like coherence, scintillation, and signal spectra (Colosi and Xu, 2007).Garrett and Munk developed an internal wave spectrum model in the 1970s, and this model has been used by many oceanographers and acousticians. This model is called the Garrett-Munk, or GM, model. Sound speed fluctuations due to internal waves are the dominant source of high-frequency variability of acoustic wave fields in the ocean (Flatte, 1975).

One of the early experiments to study sound-speed fluctuations was the MATE experiment, where the observed statistics were compared to acoustic predictions by Ewart (1984). A view of this experiment is shown in Figure (1) and Figure (2). MATE was

conducted in June and July 1977. For the MATE experiment, two receivers were placed on Cobb Seamount and one transmitter was placed on a sister seamount about 20 km from Cobb Seamount. Cobb Seamount is a volcano 275 miles west of Grays Harbor, Washington.

The MATE results involved frequencies of 2, 4, 8, and 13 kHz. Sound transmissions were sent from a single tower on one seamount to two receiving towers on Cobb Seamount over an 18.1 km range. Ewart (1984) found that the weak fluctuation theory worked well for the phase but not the intensity statistics. Spectra of the moored displacement and travel time measured during MATE are shown in Figure (3). The internal wave displacements have a frequency spectrum with power law ω-1.7 (Henvey and Ewart, 2006). Also the predicted spectrum of travel time has a power law of ω -2.7. The factor of ω difference in the power laws is a result of the Rytov theory that only IW (internal waves) whose wave numbers are perpendicular to the ray contribute to the scattering. An earlier study which was a single path experiment on Cobb Seamount had been conducted by Ewart, where observed and computational phase and intensity were within a factor of 2 (Munk and Zachariasen, 1976), but the frequency spectrum of intensity showed discrepancies. In general, early experiments conducted in the kHz region showed good agreement with phase and poor agreement with intensity. The MATE experiment results showed disagreement with Rytov theory intensity spectra in the kHz region as shown in Figure (8).

Much later, as a part of the Acoustic Thermometry of Ocean Climate (ATOC) project's Acoustic Engineering Test (AET), 75 Hz signals were transmitted to a range of 87 km with a band with of 30 Hz. Colosi and Xu (2007) examined the acoustic variability in the AET experiment, and assuming a GM (Garrett-Munk) ocean spectrum, they computed the frequency spectrum of intensity using the Rytov theory of Munk and Zachariasen (1976). The AET frequency spectrum of log-amplitude is shown in Figure (4) along with the theoretical results. The red curve is a ray angle of 10º, and the black curve is a ray angle of 5º. The solid curves are the theoretical values (Colosi and Xu , 2007). This experiment showed that the Rytov theory works at 75 Hz for the frequency

spectrum of intensity because of the weaker scattering at lower frequencies. This result provided the motivation for further study of frequencies of 75 to 400 Hz and ranges of 50 to 200 km.

The success of the weak fluctuation theory (WFT) in this low-frequency experiment has generated renewed interest in the weak fluctuation theory (WFT) as an acoustic prediction tool. This thesis addresses the limits of applicability of the Munk and Zachariasen (1976) model as a function of acoustic frequency and ray path geometry.

B. STATEMENT OF RESEARCH

The objective of this thesis is to examine efficient reduced physical models for estimating acoustic propagation through the fluctuating ocean. In particular, the goal is to be able to put error bounds on acoustic TL (transmission loss) and phase, and to predict the space-time scales of the variability for acoustic frequencies in the 75–400 Hz range. The primary research focus of this thesis is the establishment of the regimes of validity of the Rytov model as adapted by Munk and Zachariasen (Munk and Zachariasen, 1976). This addresses the important problem of characterizing the acoustic uncertainty in the ocean sound channel. For this analysis the acoustic observable of the frequency spectrum of phase and log-amplitude will be used, since many other acoustic observables, namely amplitude and phase correlation functions and coherence, can be directly derived from these spectra. Using Monte Carlo numerical simulation methods utilizing canonical models of sound speed and buoyancy frequency, this study establishes the acoustic propagation range and acoustic frequency limitations of the theory, as a function of ray path geometry.

Further, this thesis elucidates the physics leading to the breakdown of the theory. This research is a study to predict acoustic propagation statistics using “simple” analytic models rather than doing intensive and time-consuming Monte Carlo computations.

Observations of acoustic fluctuations in the ocean have been made for a number of propagation ranges, acoustic frequencies, and ray path geometry. In some cases acoustic fluctuation behavior displays features reminiscent of the weak fluctuation (Rytov) theory and in others it does not. The cause of the discrepancies in the observations may be acoustical or oceanographic in origin, that is to say the discrepancy

may be due to the fact that we do not have the correct acoustic scattering model, or it may be due to the fact that we do not have the correct ocean spectrum for sound speed fluctuations. Therefore, we have conducted a numerical experiment with a known ocean spectrum (the Garrett-Munk spectrum), and compared the full physics parabolic equation Monte Carlo simulation data to the weak fluctuation theory which also uses the GM (Garrett-Munk) spectrum. This approach directly tests the acoustic scattering model since both the numerical model and the theory have the same ocean spectrum.

Monte Carlo methods are accurate but very time-consuming; the Rytov theory, on the other hand, has a regime where it is very accurate and computationally efficient. This study provides a model for the phase and log-amplitude frequency spectra that can be used to obtain estimates of the coherence function for time separations. Important components of the coherence function are the correlation functions of the phase and log-amplitude which are related to the spectra of those quantities by Fourier Transform. This study will help to use the Rytov theory as an acoustic prediction tool and the results of this thesis will help to improve the long-range underwater communications at low acoustic frequencies.

This study focuses on internal wave effects because of the decades of strong evidence towards internal wave dominance in acoustic scattering (Colosi and Brown, 1998).

Monte Carlo numerical simulations of acoustic propagation through random fields of internal waves were carried out at acoustic frequencies of 75, 200, and 400 Hz, and we have studied the range evolutions of four acoustic ray paths to a maximum range of 200 km. Ray paths corresponding to grazing angles of 0°, 5°, 10° and 14° are considered, thus spanning the range of possible ray geometry from surface reflection to axial propagation. At a series of different ranges from the source, frequency spectra have been computed and compared to the theory to establish regimes of validity and the mechanism by which the theory breaks down. This study is limited to the effects of ocean internal waves. This study does not examine other processes like mesoscale eddies, ocean turbulence, or ocean fine structure. This study is also limited in the fact that we choose simple canonical

profiles of sound speed and buoyancy frequency: Acoustic fluctuations are known to be enhanced or degraded by various details of the background sound-speed profile (Flatte, 1983).

C. SUMMARY

This chapter introduced some of the important researchers along with their research and development in the areas of sound wave propagation through random ocean media and internal-wave-induced sound speed perturbation fields. This chapter also introduced the objective of this thesis that is to examine efficient reduced physical models for estimating acoustic propagation through the fluctuating ocean. The information that might be reached upon this study will lead to acoustic coherence information and it will be an important input for the underwater communication and sonar systems engineering studies to increase the signal-to-noise ratio and form the sonar arrays with a better understanding of the ocean sound speed field. At last, the limitations of this study are introduced.

In Chapter II, methods of analysis will be introduced. This chapter will cover the theoretical background about the internal waves (IW), Garrett-Munk (GM) spectrum and the standard parabolic equation (SPE). Chapter III will present the weak fluctuation theory of Rytov, and Chapter IV will introduce the Monte Carlo numerical simulation and split-step Fourier algorithm as a reliable tool to validate the Rytov theory. Recall that this thesis is interested in the Rytov theory of internal waves because of the dominant effects of internal waves on the sound propagation paths, and the computation speed of this theory is significantly faster than the time-consuming Monte Carlo simulations. Chapter V will present the results obtained from both the simulation and the theory and shows the theory breakpoints as the reliable regime where the theory works.

II. METHODS OF ANALYSIS

A. INTRODUCTION

This chapter presents the methods of analysis used in the computer simulations to validate the Rytov theory. We perform Monte Carlo parabolic equation simulations of sound propagation through time-evolving random realizations of internal-wave-induced sound speed field fluctuations. Some statistical quantities from these Monte Carlo calculations are compared with the Rytov theory.

The first section describes the phenomenon of ocean sound speed fluctuations induced by internal wave vertical displacements. The mathematical model developed by Garrett and Munk (C. Garrett and W. Munk, 1972) is used to characterize the internal waves in terms of their frequency/wave number spectrum. This GM (Garrett-Munk) spectrum is used to generate random realizations of internal-wave-induced sound speed fluctuations. In section B we introduce the parabolic equation method for sound propagation through arbitrary profiles of sound speed.

Before we start the theoretical development it is important to point out that this thesis uses a complex notation to present acoustic field quantities and Fourier transforms of time and space. There are some confusing quantities that have a different usage in different scientific areas, as a quantity has a different meaning in an electrical engineering text than an oceanography text. This thesis will describe its usage of these quantities mostly consistent with underwater acoustics texts. One of the quantities that differs between the electrical engineering and the underwater acoustics or oceanography texts is the direction of propagation. This thesis takes the primary direction of propagation to be in the x direction, leaving the coordinate z to be in the ocean depth direction. The y coordinate is considered to be in the transverse direction, out of the primary (x,z) plane of propagation. Another convention that has a different usage is the complex quantity $i=\sqrt{-1}$, differing from the standard electrical engineering symbol j. In this thesis the lower case j is used to define the internal wave mode number.

B. INTERNAL WAVES AND THE GARRETT - MUNK (GM) SPECTRUM

In the ocean the dominant source of the variability of acoustic fields is the sound speed fluctuations caused by internal waves (Munk and Zachariasen, 1976). Internal waves are geophysical wave motions that oscillate due to the buoyancy and Coriolis forces. Internal waves cause sound speed changes of order 1 m/s with time scales between the Coriolis period (i.e., about one day) and the buoyancy period (i.e., 10 to 20 minutes). The special scales of internal waves are of order 10 km in the horizontal and 100 m in the vertical.

Thirty-five years ago Garrett and Munk (C. Garrett and W. Munk, 1972) proposed a model synthesizing the existing observations into a model spectrum describing the distribution of observed internal wave energy in wave number and frequency space. This model has found a wide application since it is in excellent agreement with experimental observations. Energy levels generally vary by a factor of 2 and spectral slopes may vary by 10 to 20 percent.

At the basis of this theory is the fact that the ocean is stratified by density. Less dense water tends to be at deep layers of the ocean, while higher density water tends to be at shallower layers. As a consequence of this density stratification, a water parcel displaced vertically to a new depth is surrounded by a fluid with a different density, and the interplay of the buoyancy and gravity forces on the parcel leads to oscillatory motion. The character of this oscillatory motion is dictated by the buoyancy (Brunt-Väisälä) frequency *N(z)*, defined as

$$N(z) = \sqrt{\frac{-g}{\rho_0}\left(\frac{\partial \rho}{\partial z}\right)_{pot}} \quad , \tag{1}$$

where g is the acceleration of gravity (g=9.8 ms^{-2}), ρ_0 is the reference density, and $\left(\frac{\partial \rho}{\partial z}\right)_{pot}$ is the potential gradient of density. The potential gradient of density is an important quantity due to the adiabaticity of internal wave motions. The other force that acts on internal waves is the Coriolis pseudo-force whose effect is described through the

Coriolis frequency f=2 Ω sin(latitude) , where Ω is the Earth's angular velocity. Internal waves have frequencies σ between the Coriolis frequency *f* and the buoyancy frequency *N*.

Internal waves cause sound speed perturbations by vertically displacing density surfaces. Thus we can relate the sound speed *c* of a fluid parcel at depth *z*, displaced by ζ using the Taylor expansion to give

$$c(x,y,z+\zeta(\vec{r},t)) \approx \bar{c}(z) + \left(\frac{\partial \bar{c}}{\partial z}\right)_{pot} \zeta(\vec{r},t) = \bar{c}(z) + \delta c(\vec{r},t), \tag{2}$$

where *x* and *y* are horizontal coordinates, $\vec{r}$ is the position vector, $\bar{c}(z)$ is the mean sound speed profile, and *t* is time. Importantly, the sound speed perturbation δc is proportional to the potential sound speed gradient $\left(\frac{\partial \bar{c}}{\partial z}\right)_{pot}$ because of the adiabaticity of internal wave vertical displacement. The potential sound speed gradient profile can be expressed in terms of the buoyancy frequency so that the fractional sound speed fluctuation becomes

$$\mu(\vec{r},t) = \frac{\delta c(\vec{r},t)}{c_0} \approx \left(\frac{\alpha}{g}\right) N^2 \zeta \ , \tag{3}$$

where α is a dimensionless constant ($\alpha \approx 24.5$) related to the temperature and salinity relationship, c_0 is a reference sound speed equal to 1500 m/s, and *N* is the buoyancy frequency.

Equation (3) can be used to understand the statistics of internal wave induced sound speed fluctuations. The variance of $\mu(\vec{r},t)$ can be written as (Flatte et al., 1979)

$$\left\langle \mu^2 \right\rangle (z) = \mu_0^2 \frac{N^3(z)}{N_0^3}, \tag{4}$$

where μ_0^2 is a reference fractional sound speed variance taken to be $\mu_0^2 = 6.26 \times 10^{-8}$ and N_0 is a reference buoyancy frequency taken to be 3 cph (cycles per hour). This equation gives us an important result. It shows that internal-wave-induced sound speed

fluctuations are inhomogeneous in depth. Since in the upper ocean the buoyancy frequency is much larger than in the deep ocean, internal-wave-induced sound speed fluctuations are much larger in the upper ocean.

Internal waves in the ocean can be represented as horizontally propagating vertical modes. Therefore the internal wave displacement field ζ can be considered as a sum over all possible internal waves with wave numbers k_x, k_y and vertical mode number j, such that (Colosi, 2005)

$$\zeta(x,y,z,t) = \mathrm{Re}[\int_{-\infty}^{\infty}\int_{-\infty}^{\infty} dk_x dk_y \sum_{j=1}^{\infty} g(j,k_x,k_y) A_j(z,k_h) e^{i(k_x x + k_y y - \sigma_j(k_h)t)}], \quad (5)$$

where $k_h = \sqrt{k_x^2 + k_y^2}$ is the horizontal wave number, A_j is the jth mode function, and $\sigma_j(k_h)$ is the dispersion relation. The amplitudes of each of these internal waves $g(j,k_x,k_y)$ are considered to be complex random variables whose statistics are described by the Garrett-Munk (GM) spectrum. According to the GM spectrum, the internal wave amplitudes are independent zero mean complex Gaussian random variables such that

$$\langle g(j,k_x,k_y) g^*(j',k'_x,k'_y)\rangle = G_\zeta(j,k_x,k_y)\delta(k_x - k'_x)\delta(k_y - k'_y)\delta(j-j'), \quad (6)$$

where $G_\zeta(j,k_x,k_y)$ is the internal wave (IW) spectrum and * denotes the conjugate operation.

The Garrett-Munk spectrum as a function of mode number and frequency is given by

$$G_\zeta(j,\sigma) = \frac{4}{\pi}\frac{1}{M}\zeta_0^2 \frac{N_0}{N(z)}\frac{f\sqrt{(\sigma^2 - f^2)}}{\sigma^3}\frac{1}{j^2 + j_*^2}, \quad (7)$$

where the mode bandwidth j_* =3 is a constant, and $M = \sum_{j=1}^{\infty}\frac{1}{j^2 + j_*^2}$ is a normalization. The spectrum is normalized such that

$$\sum_{j=1}^{\infty}\int_{f}^{\infty} G_{\zeta}(j,\sigma)d\sigma = \left\langle \zeta^2 \right\rangle (z) = \zeta_0^2 \frac{N_0}{N(z)}, \tag{8}$$

where ζ_0 is a reference internal wave displacement. Particularly important is the spectrum of μ, thus modifying the normalization the spectrum of μ is

$$G_{\mu}(j,\sigma) = \frac{4}{\pi}\frac{1}{M}\mu_0^2 \frac{N^3(z)}{N^3{}_0}\frac{f\sqrt{(\sigma^2 - f^2)}}{\sigma^3}\frac{1}{j^2 + j_*^2}. \tag{9}$$

To get a random realization of μ via Equation (5), the spectrum must be given in terms of the mode number *j* and horizontal wave numbers k_x and k_y. The coordinates have been changed in Equation (9) using the WKB dispersion relation (Colosi and Xu, 2007),

$$\sigma^2 = f^2 + \frac{\left(k_x^2 + k_y^2\right)}{k_z^2}N^2(z), \tag{10}$$

where $k_z = \frac{\pi j N(z)}{N_0 B}$, $N_0 B = \int_0^D N(z)dz$ and *D* is the water depth. The result is

$$G_{\mu}(j,k_x,k_y) = \mu_0^2 \frac{N^3(z)}{N_0^3}\frac{1}{M}\frac{1}{j^2 + j_*^2}\frac{2}{\pi^2}\frac{k_j\sqrt{k_x^2 + k_y^2}}{\left(k_x^2 + k_y^2 + k_j^2\right)^2}, \tag{11}$$

where $k_j = \frac{f\pi j}{N_0 B}$.

In the ocean, the buoyancy frequency is approximately $N(z) \approx N_s e^{-z/B}$, where the surface buoyancy frequency is $N_s \approx 5cph$ and thermo cline depth is $B \approx 1000m$. As previously noted, internal waves are inhomogeneous in depth since the variance $\left\langle \mu^2 \right\rangle$ of the relative speed change is larger near the ocean surface. Also of importance, the spectrum given by Equation (11) is isotropic in the horizontal direction (i.e., only depends on $k_x^2 + k_y^2$). On the other hand, internal waves are anisotropic in the vertical-horizontal direction. Vertical scales are roughly 0.1 km, while horizontal scales are roughly 10 km.

C. PARABOLIC EQUATION

The method of parabolic wave equations was first introduced by Leontovich and Fock (1946) and applied to a radio wave propagation problem in the atmosphere (Jensen, Kuperman, Porter & Schmidt, 2000). The parabolic equation (PE) method has found wide application in the field of underwater acoustics after Hardin and Tappert (1973) devised an efficient model based on Fourier transforms. The PE method has become the most popular method to solve range-dependent ocean wave propagation problems.

In this thesis, the derivation of the parabolic equation follows the treatment by Jensen, Kuperman, Porter & Schmidt (2000). There are different kinds of parabolic equations, but this thesis will be using the so-called standard parabolic equation, which is the crudest approximation for small angle forward scattering. This is also the approximation made in the Rytov theory.

1. Standard Parabolic Equation

Sound propagation through a spatially variable and time-evolving ocean is described by the acoustic wave equation given by

$$\nabla^2 p(\vec{r},t) = \frac{1}{c^2(\vec{r},t)} \frac{\partial^2 p}{\partial t^2}. \tag{12}$$

However, the ocean time scales of variability are much longer than an acoustic wave period and thus the sound speed can be considered frozen in time during the passage of an acoustical wave. Therefore, in Equation (12) the time dependence of the sound speed $c(\vec{r},t)$ can be neglected, and the Helmholtz equation can be examined for a harmonic point source of time dependency (exp (-iωt)) in cylindrical coordinates (r, φ,z) where two-dimensional propagation is assumed in the (r,z) plane. The time evolution of the internal wave sound speed field will be treated by specifying the individual frozen sound speed fields as $c(r,z,t_m)$, where t_m is the internal wave evolution time. The Helmholtz equation is therefore

$$\nabla^2 p + \frac{\omega^2}{c^2} p = \frac{\partial^2 p}{\partial r^2} + \frac{1}{r}\frac{\partial p}{\partial r} + \frac{\partial^2 p}{\partial z^2} + k_0^2 n^2 p = 0 \ , \text{ (Cylindrical coordinates).} \tag{13}$$

where $p(r,z,t_m)$ is the acoustic pressure, ω is the radial frequency, $k_0 = \frac{w}{c_0}$ *i*s a reference wave number, and $n(r,z,t_m) = \frac{c_0}{c(r,z,t_m)} \approx \frac{c_0}{\bar{c}(z)} - \mu(r,z,t_m)$ is the index of refraction. The sound speed is

$$c(r,z,t_m) = \bar{c}(z) + \delta c(r,z,t_m). \tag{14}$$

The acoustic pressure can be written as

$$p(r,z) = \psi(r,z) H_0^{(1)}(k_0 r), \tag{15}$$

where ψ is the complex wave amplitude, $H_0^{(1)}(k_0 r)$ is a Hankel function of the first kind, and $H_0^{(1)}(k_0 r) \approx \sqrt{\frac{2}{\pi k r}} e^{i(kr - \pi/4)}$. Substituting Equation (12) into Equation (11) and making the small angle approximation,

$$\frac{\partial^2 \psi}{\partial r^2} \approx 2ik_0 \frac{\partial \psi}{\partial r}, \tag{16}$$

gives the standard parabolic equation (Hardin and Tappert,1973):

$$2ik_0 \frac{\partial \psi}{\partial r} + \frac{\partial^2 \psi}{\partial z^2} + k_0^2 (n^2 - 1)\psi = 0, \tag{17}$$

where n is the index of refraction.

This equation will be used with random realizations of internal waves to perform Monte Carlo numerical simulations.

D. SUMMARY

This chapter introduced the basic physical concepts such as the definition of internal waves and the Garrett-Munk spectrum and also the parabolic equation. This thesis focuses on finding the regions of validity of the Rytov theory using Monte Carlo simulations. In the next chapter, weak fluctuation theory (Rytov theory) for the random ocean media will be presented, and the following chapter will describe the Monte Carlo numerical simulation.

THIS PAGE INTENTIONALLY LEFT BLANK

III. WEAK FLUCTUATION THEORY (RYTOV THEORY)

A. INTRODUCTION

This chapter presents the Rytov theory applied to ocean acoustic propagation through random internal-wave-induced sound speed perturbations obeying the GM (Garrett-Munk) internal wave spectrum. The theory gives the spectra of log-amplitude and phase for individual ray paths that traverse the ocean waveguide at various grazing angles (i.e., ray angle at the sound channel axis). The physical model under consideration is that of weak, small-angle, multiple forward scattering. The parameters used to analyze the regimes of validity of the weak fluctuation theory of Rytov will be described. When the regions of validity of the weak fluctuation theory are defined and the physics behind the breakdown points described, the Rytov theory will help ocean acousticians better understand the stability of ocean acoustic wave fields. This effort will aid in the development of new and better systems for acoustic remote sensing, communications, and navigation.

B. RYTOV THEORY

The Rytov theory treats the physical situation of weak, small-angle forward scattering, where phase fluctuations lead to intensity fluctuations. Figure (5) shows how phase fronts are distorted by sound speed heterogeneities leading to focusing and defocusing. Conceptually, the Rytov theory reveals a resonance condition such that only internal waves whose wave numbers are perpendicular to the sloping ray contribute to the scattering. Figure (6) shows the geometry of this ray internal wave interaction. In this figure, (+) indicates the areas with higher speed and (-) indicates the areas with lower speed. In this case the acoustic wave front is distorted, leading to focusing and defocusing. On the other hand, internal waves whose wave numbers are parallel to the ray phase front do not lead to wave front distortion and thus do not contribute strongly to the acoustic scattering [See Figure (7)]. An example of the effect of internal waves on acoustic beam propagation is shown in Figure (9). This figure shows an unperturbed ray beam at 200 Hz and 5° launch angles in the upper plot and the perturbed ray beam in the lower plot. The beam is distorted, leading to focusing and defocusing. We also see that

the unperturbed beam is broken up into many smaller beams and that interference effects can be strong.

This paper uses the treatment of Munk and Zachariasen (1976) and also Colosi and Xu (2007) in applying the Rytov method to internal-wave-induced acoustic fluctuations in an ocean waveguide. Background buoyancy frequency and sound speed profiles are dependent only on the depth coordinate z where $c=\bar{c}(z)$ and $N=N(z)$. An important aspect of ocean acoustic propagation with an ocean waveguide with $c=\bar{c}(z)$ is that the unperturbed ray paths are curved. The Rytov theory was originally developed to describe optical propagation through a turbulent atmosphere. In this case the unperturbed ray paths are straight lines. The Rytov formulations of Munk and Zachariasen (1976) and Colosi and Xu (2007) are shown to be local applications of the straight ray results; thus the theory can break down if the ray has significant curvature. The results of this thesis will show aspects of this breakdown for the steepest rays considered.

Weak fluctuation theory is known to be valid for small intensity fluctuations where the variance of log-amplitude $\langle \chi^2 \rangle \ll 1$ scintillation index (SI) is approximately less than or equal to $0.3-0.4$, and $\sigma_{\ln I}$ is approximately less than or equal to 1 to 2 dB. Phase statistics are expected to be valid where variance of phase is $\langle \phi^2 \rangle \geq (2\pi)^2$.

Following the derivations from Colosi and Xu (2007), the frequency wave number spectra of phase ϕ and log-amplitude χ at range R for a given ray path Γ are

$$F_{\phi,\chi}(R,\omega,k_z(j)) = \pi k_0^2 R \int_\Gamma ds G_\mu(0,\omega,k_z(j);z)\left[1 \pm \cos\left(\frac{k_z^2 R_{fz}^2(x)}{2\pi}\right)\right], \qquad (18)$$

where $(+)$ corresponds to ϕ and $(-)$ corresponds to χ in the second term of the integral. In other words, this integral will give the frequency wave number spectrum of phase if (+) is used in the second term, and it will give frequency wave number spectrum of log-amplitude if (-) is used in the second term. This integral shows the relation between frequency spectrum of phase and frequency spectrum of log-amplitude. Importantly, the integral in Equation (18) is along a specific ray path of the unperturbed

sound speed profile; the parameter Γ then gives the coordinates of the ray path $z_r(x)$. Integration over specific ray paths is significant here, because the distinct ray paths sample the inhomogeneous and anisotropic internal wave field differently; a ray traveling down the sound channel axis at zero grazing angle will see a different internal wave field than one that reflects off the sea surface and has a relatively large grazing angle. This integral has two important terms that will be discussed next. There is a spectral term denoted by *G(0,w,kz)* and a diffraction term given by $\left[1 \pm \cos\left(\frac{k_z^2 R_{fz}^2(x)}{2\pi}\right)\right]$.

The first term is the spectrum of sound speed fluctuations, where the perpendicular wave number constraint has been applied. The GM (Garrett and Munk) spectrum with perpendicular wave number constraint is given by

$$G_\mu(0,\omega,k_z(j);z) = \frac{\mu_0^2 N^3}{N_0^3}\frac{8}{\pi^3}\frac{k_{z_*}}{k_z(k_z^2+k_{z_*}^2)}\frac{Nf}{\omega^3}\left(\frac{\omega^2-f^2}{\omega^2-\omega_L^2}\right)^{1/2}, \ \omega_L < \omega < \mathrm{N}, \qquad (19)$$

where it is valid for the frequencies ω between the cutoff frequency ω_L (the lower limit) and the buoyancy frequency *N*. The origin of the lower frequency cutoff ω_L is discussed in what follows. The component of the internal wave perpendicular to a ray with slope $\theta(z_r(x))$ is

$$k_\perp(z_r(x)) = (-k_z \tan\theta(z_r(x)), k_y, k_z), \qquad (20)$$

where $z_r(x)$ is the depth of the unperturbed ray path. The internal wave dispersion relation in the WKB limit with the perpendicular wave number constraint is (Colosi and Xu, 2007)

$$k_h = \sqrt{k_z^2 \tan^2(\theta) + k_y^2} \approx \frac{\pi j}{N_0 B}(\omega^2 - f^2)^{1/2}, \qquad (21)$$

where ω is the internal wave frequency and *f* is the Coriolis parameter. If we solve this equation for k_y then

$$k_y = \frac{\pi j}{N_0 B}\sqrt{(\omega^2-\omega_L^2)}, \qquad (22)$$

$$\omega_L^2 = f^2 + N^2 \tan^2 \theta \,, \tag{23}$$

where ω_L is IW lower frequency (cutoff) limit. This equation shows that if $\omega \le \omega_L$ then k_y cannot be a real number and dispersion relation cannot be satisfied for internal wave frequencies less than ω_L. Thus, internal waves whose frequencies are less than the lower frequency limits ω_L do not interact with the acoustic field locally.

The second term in Equation (18), which is in square brackets, is the Fresnel filter. $R_{fz}^2(x)$ is the vertical Fresnel zone (Flatte et al., 1979). The Fresnel filter can be considered as a weighting function on the spectrum which controls the contributions to the phase and log-amplitude variances at each wave number k_z. This filter function accounts for effects of diffraction. The spectra $F_{\phi,\chi}(R, w, kz)$ mirrors the ocean spectrum of sound speed except for the action of the filter function. The Fresnel filter has its maximum at k_z=0 for phase. Considering the fact that the internal wave spectrum at perpendicular wave number is approximately k_z^{-3}, variance of phase is most sensitive to large scales of the spectrum (i.e., where k_z is small). The Fresnel filter has its first maximum for when

$$\cos\left(\frac{\left|k_\perp\right|^2 R_f^2(x)}{2\pi}\right) \to -1 \quad \text{or} \tag{24}$$

$$\frac{\left|k_\perp\right|^2 R_f^2}{2\pi} \to \pi \,, \quad \left|k_\perp\right| \to \frac{\sqrt{2}\pi}{R_f} \quad . \tag{25}$$

Thus log-amplitude fluctuations are most sensitive to internal wave scales near the Fresnel zone. For the situation in which there is no waveguide, the Fresnel zone is given by $R_f^2(x) = \lambda x \frac{(R-x)}{R}$, where λ is the acoustic wavelength, and R is the range. Conceptually, the Fresnel zone describes a diffractive region or zone around a geometric ray path (Flatte et al., 1979). In this thesis the Fresnel zone in the ocean waveguide is

computed using the methods in Colosi and Xu (2007). It is important to note that this computation does not handle the Fresnel zone properly when the ray gets near the ocean surface.

Important acoustic observables are the frequency spectrum of phase and the phase variance

$$F_\phi(w) = \int_{-\infty}^{\infty} F_\phi(k_z, \omega) dkz, \left\langle \phi^2 \right\rangle = \int_{-\infty}^{\infty} \int_{w_L}^{N} F_\phi(k_z, \omega) dkz d\omega \quad . \tag{26}$$

We will use this equation to calculate the phase spectra and variance for the Rytov theory, and, importantly, we will analyze the phase variance from the Rytov theory with the phase variance from Monte Carlo numerical simulations as shown in Figure (13).

The log-amplitude frequency spectrum and variance is

$$F_\chi(w) = \int_{-\infty}^{\infty} F_\chi(k_z, \omega) dkz, \left\langle \chi^2 \right\rangle = \int_{-\infty}^{\infty} \int_{w_L}^{N} F_\chi(k_z, \omega) dkz d\omega \quad . \tag{27}$$

Equation (27) will be used to calculate the log-amplitude frequency spectrum and variance for the Rytov theory, and importantly, we will analyze the log-amplitude variance from the Rytov theory with the log-amplitude variance from Monte Carlo numerical simulations as shown in Figure (14). Log-amplitude variance is important to calculate the transmission loss in the ocean.

The main approximations of the Rytov theory are:

1) Ray curvature is small; equations assume a locally straight ray. That is to say the ray cannot change orientation within an internal wave correlation length. This condition breaks down for all rays at the turning point of maximum curvature.

2) Single scattering (perturbation theory is only taken to first order).

3) Expansion about the unperturbed ray. This study integrates the Rytov equations over the unperturbed ray path. Internal waves do make the unperturbed ray path unstable, but the instability range seems to be in the range 200–500 km.

4) Fresnel zone: This study Computes the Fresnel zone, again using the unperturbed ray. Internal waves may in fact modify the Fresnel zone. We also do not take into account the ocean surface boundary condition when we compute the Fresnel zone.

C. SUMMARY

This chapter described the weak fluctuation theory of internal waves and the important parameters that will be used for analyzing the Monte Carlo simulation with the Rytov theory. In this chapter the findings of earlier studies about Rytov theory were given. One of the important points described in this chapter was the usage of the Munk and Zachariasen (1976) treatment. In this approach, straight ray formulas are used locally, and this approximation breaks down for significant curvatures. Dispersion relation cannot be used for frequencies of variability less than cutoff frequency ω_L. The Rytov theory says that only internal waves with perpendicular wave numbers contribute to the scattering. Phase is most sensitive to large scales of the spectrum. Log-amplitude is most sensitive to the scales near the Fresnel zone. The approximations used in this theory were given at the end of this chapter.

This thesis uses the approximations given in this chapter, and the results chapter will show where the Rytov theory breaks down due to these approximations. In the conclusions chapter, the reasons for the theory's breakdown points and future recommendations for follow-on work will be discussed.

The next chapter will present the Monte Carlo numerical simulation. It is the most reliable method, but is very time consuming.

IV. MONTE CARLO NUMERICAL SIMULATION

A. INTRODUCTION

This chapter presents the Monte Carlo numerical simulation, which is known to be the most reliable and accurate method to validate the weak fluctuation theory of Rytov. The Garrett-Munk ocean spectrum is used for both the Monte Carlo numerical simulation and the Rytov theory and was presented in Section 2. This chapter introduces the sound speed field and the model parameters chosen for the simulation and the split-step Fourier algorithm. One simulation was made for the phase variance and log-amplitude variance calculated with independent random realizations. Another simulation was made for phase and log-amplitude spectra executed with time evolution of 1 realization. The results from the simulation will be presented in the next chapter.

B. SOUND SPEED FIELD AND MODEL PARAMETERS

In this thesis the background environment is a Munk canonical profile (Munk, 1974) as seen in Figure (11). The analytic form of the Munk profile is

$$\overline{c}(z) = c_0\left[1+\varepsilon(e^{-2(z-z_a)/B}+2(z-z_a)/B-1)\right] , \tag{28}$$

where B is the thermo cline depth scale, the minimum mean sound speed c_0 is 1500 (m/s), the sound channel axial depth z_a is 1000 m, the total water depth is 5000 m, and $\varepsilon = 0.005515$ is the perturbation coefficient, which is a dimensionless constant.

The sound speed field used in this paper is a two-dimensional sound speed field dependent on x and z coordinates consisting of a mean sound speed profile and sound speed perturbations dependent on the location and time such that

$$c(x,z) = \overline{c}(z) + \delta c(x,z,t) \ . \tag{29}$$

Realizations of sound speed perturbations are generated by the method of Brown and Colosi (1996), as described in Section 2.

C. PARABOLIC EQUATION METHOD

1. Split-Step Fourier Algorithm

Since Hardin and Tappert (1973) introduced the split-step Fourier method for solving the parabolic equation to the underwater acoustic community, this method has found wide application. This study uses the split-step Fourier algorithm shown by Jensen et al., (2000):

$$\Psi(r,z) = F^{-1}\left\{ e^{-\frac{i\Delta r}{2k_0}k_z^2} F\left\{ e^{\frac{ik_0}{2}\left[n^2(r_0,z)-1\right]\Delta r} \Psi(r_0,z) \right\} \right\}, \tag{30}$$

where r_0 and r are two different ranges separated by the increment $\Delta r = r - r_0$ at each step, the capital letter "F" is the Fourier transform from the z domain to the k_z domain, and the symbol "F^{-1}" is the inverse Fourier transform. This algorithm starts with marching the solution out in range with a phase screen. This phase screen takes the refractive effects into account. The next step is advancing the solution for a homogeneous medium to include diffraction (Jensen et al.,, 2000). The split-step Fourier algorithm parameters are given in the first three columns of Table 1:

Frequency (Hz)	dx (m.)	dz (m.) , (N)	θ_1 (deg)	θ_2 (deg)	Maximum time evolution
75	50	2.4414 , (2048)	0.75	(0,5,10,14)	10 days
200	20	2.4414 , (2048)	3.75	(0,5,10,14)	20 days
400	10	1.2207 , (4096)	3.75	(0,5,10,14)	7.5 days

Table 1. Split-step algorithm parameters

where *dx* is the split-step range interval length, *dz* is the depth grid spacing, and *N* is the number of depth grids.

The values for *dx* and *dz* were chosen to compromise between accuracy and simulation time. For greater values of *dx* and *dz* the Monte Carlo numerical simulation runs faster while loosing accuracy, while for smaller values of *dx* and *dz* the simulation yields more accurate results at the expense of a considerable increase in simulation time.

Different values of *dx* and *dz* were tested in a number of short realizations in order to set the parameters for the right accuracy. Then the number of grids was set based on the fact that the maximum depth is 5000 m and the number of grids is equal to the maximum depth divided by the depth grid spacing (N=5000/dz). Furthermore, the accuracy of the results is influenced by the beam width. Since waves at 200 and 400 Hz have a wider beam than waves at 75 Hz, the latter yields results with better resolution.

Two different simulations were carried out. The first one was for phase variance and log-amplitude variance, which was executed with independent random realizations. And the second simulation was for phase and log-amplitude spectra executed with time evolution of 1 realization.

2. Boundary and Initial Conditions

This study used the parabolic equation method to simulate an image ocean. An image ocean is simulated to treat the ocean surface as a reflecting boundary (pressure release) which translates to the boundary condition $\Psi(r,z)=0$.

The boundary condition can be satisfied by subtracting the image source, which is created in the reflected image ocean, from the source at depth z_s (Jensen et al.,, 2000).

$$\Psi(0,z)=\Psi(0,z-z_s)-\Psi(0,z+z_s) \tag{31}$$

The boundary condition at the bottom of the ocean is treated by an attenuation function, or "sponge layer" due to the periodic boundary conditions of FFT (Fast Fourier Transform) solution. This absorption layer is used to prevent the waves from entering the domain at the top after they exit from bottom. If there weren't any absorption layer, the periodic FFT solutions would be mistaken by the waves which should be absorbed. Colosi and Flatte (1996) produced a sponge layer to avoid this wrap-around problem, expressed as

$$L(z)=\exp\left\{-\beta dx\times\exp\left(-\left(\frac{z-z_b}{\alpha z_b}\right)^2\right)\right\} \quad , \tag{32}$$

where z_b is the bottom depth of computational domain, β is the relative strength of the loss and chosen to be $\beta = 0.04$, and α is the loss relative to the bottom and chosen to be $\alpha = 0.05$.

For the narrowband simulation, a directional source is modeled (Colosi, 2007) as

$$\psi(x=0,z) = k_0^{1/2} \tan(\theta_1) \exp\left(\frac{-k_0^2 \tan^2(\theta_1(z-z_s))}{2} \right) \exp\left(ik_0 \sin\theta_2 (z-z_s) \right), \qquad (33)$$

where k_0 is the reference wave number, z_s is the source depth, θ_1 is the beam width, and θ_2 is the beam angle. Table 1 gives the beam parameters for the various simulations that were done.

3. Phase and Amplitude Fluctuations

In this section the symbol $'$ is used for defining perturbed quantities, and the subscript $_0$ is used to define the unperturbed quantities. For example, the quantity a' is the perturbed amplitude with sound speed fluctuations, and a_0 is the unperturbed amplitude. The perturbed field pressure is thus written

$$\Psi' = a' e^{i\phi'} = e^{\chi' + i\phi'}, \qquad (34)$$

and the unperturbed field pressure is

$$\hat{\Psi} = a_0 e^{i\phi_0} = e^{\chi_0 + i\phi_0}, \qquad (35)$$

where the log-amplitude is defined as $\chi = \ln a$, ϕ_0 is the unperturbed phase, and the perturbed phase is $\phi' = \phi_0 + \phi$. The phase fluctuation and log-amplitude fluctuation can be found by dividing the perturbed field pressure by the unperturbed field,

$$\frac{\psi'}{\hat{\psi}} = e^{\chi' - \chi_0} e^{i(\phi' - \phi_0)} = \frac{a'}{a_0} e^{i\phi}, \qquad (36)$$

which will lead to the phase fluctuation taking the imaginary part of the natural log of the ratio of perturbed field over unperturbed,

$$\phi = \mathrm{Im}\left(\ln \frac{\psi'}{\hat{\psi}} \right), \tag{37}$$

and the log-amplitude fluctuation is the difference between the perturbed log-amplitude χ' and unperturbed log-amplitude χ_0. Log-amplitude fluctuation can be defined as the real part of the ratio of the perturbed sound speed field divided by the unperturbed field,

$$\chi' - \chi_0 = \mathrm{Re}\left(\ln \frac{\psi'}{\hat{\psi}} \right) = \ln \frac{a'}{a_0} \quad . \tag{38}$$

It is important to note that in the simulation, which is not broadband, the phase ϕ will be between 0 and 2π. To compute phase statistics, the phase must be unwrapped. For the time-evolving internal wave simulations, this is possible because there is phase information as a function of both range and time along the beam; that is $\phi(x,t)$. In this case a two-dimensional phase unwrapping technique can be applied (Colosi et al., 2004). For the Monte Carlo simulations with independent internal wave realization used to quantify phase variance, there are independent realizations of phase as a function of range only; that is $\phi(x)$. Hence the phase may only be unwrapped in the *x* direction. In 1-D phase unwrapping, problems can occur when the intensity gets small and phase becomes ill defined.

D. SUMMARY

In this chapter, two different Monte Carlo numerical simulations were carried out to find the validity regions of the Rytov theory. The first simulation was to investigate both phase and log-amplitude variances by executing independent random realizations of the numerical simulation. The second, larger simulation was to compute phase and log-amplitude frequency spectra from time series of complex pressure. Here the acoustic pressure field was simulated every two minutes for multiple days. Due to the time-consuming nature of this calculation, only one realization of the internal wave random amplitudes was time-evolved. As previously mentioned these simulations are very time consuming. For example, for the 200 Hz calculation, it was necessary to simulate 20 days of internal wave time evolution, and this calculation took close to 20 days! The 75 Hz

calculation took a little less time, while the 400 Hz calculation took slightly more time. By comparison, the use of the Rytov theory reduced the computation time to a few minutes in all cases.

The simulations also were very memory intensive and disk space intensive; the random internal wave realizations required 2 GB of RAM, while almost 500 GB of hard drive space was used. On the other hand, the computational requirements for the Rytov theory are inconsequential.

In the next chapter the regions of validity and the breakpoints of the Rytov theory will be presented. This will introduce new regions where the time and computer memory could be saved.

V. RESULTS

This chapter presents the results for the phase and intensity variance, and the phase and intensity spectra. Beam angles of 0º, 5º, 10º, and 14º and acoustic frequencies of 75, 200 and 400 Hz are considered. The results are illustrated with the figures showing the Monte Carlo numerical simulation and the Rytov theory results in the same display. These results will extend the usage of the weak fluctuation theory of Rytov. The success of the weak fluctuation theory at low acoustic frequencies will increase the interest of this theory. These results show the validity limits of the Rytov theory where many applications in underwater communications and signal processing for underwater acoustics can be used.

A. PHASE VARIANCE

In this paper we start analyzing the results by looking at the phase variance and comparing the Rytov theory with simulation. Figure (13) shows the results with subplots for each launch angle (0°, 5°, 10°, 14°) that we are analyzing in this paper. Each subplot has different colors for different frequencies. 75 Hz is shown with red, 200 Hz is shown as green, and 400 Hz is shown with blue. The simulation data is shown with solid lines and the theory is shown with dashed lines. Rms values of phase variance (rad) are plotted for up to 200 km range. For many of the phase statistics at higher frequencies and longer ranges, estimates could not be made because fade-outs prevented accurate phase unwrapping as discussed in Chapter V.

At 0° launch angles the Rytov theory works very well for 75 Hz, but it gets worse for higher frequencies. All results show the same pattern with an increasing rms value changing like $R^{1/2}$.

The theory also works very well for 5° launch angles at 75 Hz up to the maximum simulated range of 200 km. At about 50 km the error is almost 25%, but the difference from the simulation results gets larger with range. At 200 km the difference is more than 50% of the simulation. At 400 Hz the standard deviation of the phase increases faster than it does at 75 Hz and 200 Hz. The simulation is almost twice the theory on average. The theory for 400 Hz is better at 50 km and it gets worse with increasing range.

At 10° and 75 Hz the theory is still giving a very good estimate close to the simulation and the estimation error is less than 20%. The theory is also working well at 200 Hz and a 10° launch angle. Theoretical values are increasing parallel to the simulation values with less than 30% difference. At 400 Hz the theory is almost 50% of the simulation, although both the theory and simulation show increasing error with increasing range.

At 14° all the results for phase variance show that the theory cannot predict accurately at this higher launch angle. It can be generalized that the theory breaks down after 10° for these frequencies. The theory breaks down because of the surface interaction.

B. INTENSITY VARIANCE

This analysis continues by examining the rms fluctuation of log-intensity. Figure (14) shows the intensity fluctuations in dB for 75, 200, and 400 Hz acoustic frequencies for beam angles of 0°, 5°, 10° and 14°. As in Figure (13), different acoustic frequencies are separated with different colors, and solid lines show simulation data while dashed lines show theoretical results.

At 0°, theoretical results at 200 Hz and 400 Hz match the simulation with a very small difference. Although the theoretical data for 200 Hz and 400 Hz is in good agreement with simulation, the data at 75 Hz data is not as good. Here the difference is less than 1 dB and the shapes of the curves are very similar.

At 5°, the theory predicts 75 Hz data better than at 0°, but this time the theoretical results are less than 0.5 dB higher than simulation data. At 5°, the theory also predicts the 200 Hz data quite well. The theory does not predict the 400 Hz data quite as well as data for 75 and 200 Hz, but the error is still less than 40%. The theory predicts the intensity fluctuations adequately out to the maximum range of 200 km.

For the 10° beam, the theory predicts the 75 Hz data very well, except for the large spikes. The spikes occur at turning points where the mean intensity is low. The 10° results are worse at 200 Hz and the 400 Hz results are worse still. Thus, the theory seems to break down for higher frequencies at 10°.

The results for the 14° beam in Figure (14) clearly show that the theory breaks down at this high angle.

In summary, these results for the intensity fluctuations show that the Rytov theory provides a good prediction up to 5° for all three frequencies. The theory also gives a good prediction at 10° and 75 Hz . The theory breaks down after 10° for all three frequencies.

C. PHASE SPECTRA

In this section we will analyze the frequency spectra of phase. The next section will discuss the frequency spectra of log-amplitude. As before, the analysis is made for 12 cases, with 3 different frequencies of 75, 200, and 400 Hz, and for each frequency, 4 different grazing angles of 0°, 5°, 10° and 14°. Results are plotted for the 12 cases, starting from Figure (15) for 75 Hz and 0° grazing angle and ending with Figure (26) for 400 Hz and 14° angle. In this section the important idea is to compare the shapes of the spectra, as the variances were already discussed in sections A and B.

In these figures, the red curves are the spectra of phase S_ϕ from the Monte Carlo simulation, and the blue curves are spectra from the Rytov theory. The green curve is the μ spectra from the internal wave simulation. The spectra of μ are shown to demonstrate the cutoffs at f and N and to show the ω^{-2} form. We will compare the theoretical results with the Monte Carlo simulation. Each figure has the theoretical value for phase variance on the title. Ranges used for different launch angles are given in Table 2. These ranges were chosen to be very nearly after the beam traversed an upper turning point.

Launch Angle	Range (km.) 1st subplot	Range (km.) 2nd subplot	Range (km.) 3rd subplot	Range (km.) 4th subplot
0°	50	100	150	200
5°	62	106	152	200
10°	68	120	172	200
14°	70	130	190	200

Table 2. Ranges used for different launch angles in each subplot

1. Spectral Energy at 75 Hz

Figure (15) shows the phase spectrum of the theory and the simulation at 75 Hz and 0° launch angles at the predefined ranges seen in Table 2. The theory is in good agreement with the simulation except for 200 km at low frequencies of variability, where theory predicts more energy than observed in the simulation.

Figure (16) shows the phase spectrum of the theory and the simulation at 75 Hz and 5° launch angles at the predefined ranges seen in Table 2. The theory is generally in good agreement with the simulation, but at the lowest frequencies of variability the theory slightly overpredicts the level of the spectrum. Importantly, both the theory and simulation show a change in spectral slope at roughly 0.2 cph. For frequencies greater than 0.2 cph, the slope is very nearly ω^{-3}, whereas for lower frequencies of variability the slope is less. This break in slope is caused by the Rytov resonance condition in which internal waves whose wave numbers are perpendicular to the ray limit the influence of low-frequency internal waves.

Figure (17) shows the phase spectrum of the theory and simulation at 75 Hz and 10° launch angles at the predefined ranges seen in Table 2. The spectral comparisons for the 10º ray are very similar to the ones for the 5º ray. The theory predicts the spectrum of the phase very well at all ranges and frequencies of variability (cph) at 75 Hz and 10°. As before, the theory slightly overpredicts the spectral energy at lower frequencies of variability. In this case, however, because we have a steeper ray, the change in slope of the spectrum occurs at about 0.5 cph.

Figure (18) shows the phase spectrum of the theory and simulation at 75 Hz and 14° launch angles at the predefined ranges seen in Table 2. We see dramatic differences between the theory and the simulation for the 14º ray. Recall that the 14º ray beam has significant surface interaction and thus it has more complex ray geometry. The theory significantly underpredicts the spectral energy level at frequencies of variability less than 1 cph. At the same time, the theory is relatively accurate for frequencies of variability greater than 1 cph. In this frequency of variability range the spectrum very nearly has ω^{-3} shape. At the 14º ray we observed a very significant effect of ω_{L} (cutoff frequency) on the spectrum for frequencies less than 1 cph. Recall that ω_{L} limits the spectral

contributions from the low-frequency internal waves. The simulation shows more spectral energy at low frequencies of variability than the theory, because the surface interaction seems to have modified the Rytov resonance condition in which only perpendicular wave numbers contribute. An important further study would be to understand the breakdown of the theory in this regime.

2. Spectral Energy at 200 Hz

Figure (19) shows the phase spectrum of the theory and simulation at 200 Hz and 0° launch angles at the predefined ranges seen in Table 2. We observed very good agreement with the Rytov theory between the buoyancy frequency and the inertial frequency in which ω^{-3} spectral form is readily observed. However, for the larger ranges there is significant spectral energy at the frequencies of variability greater than the buoyancy frequency. In particular, at 200 km range the ω^{-3} shape continues all the way to the highest frequency of variability of 20 cph. The appearance of this energy at high frequency is due to interference effects. The Rytov theory does not predict this energy, because the Rytov theory is based on the internal wave dominance, and the highest possible frequency of internal wave is the buoyancy frequency. Because of this approach, the interference and scattering where $\omega > N$ is not treated in the weak fluctuation theory (Rytov theory). This effect should be a further study to investigate.

Figure (20) shows the phase spectrum of the theory and simulation at 200 Hz and 5° launch angles at the predefined ranges seen in Table 2. The theory and simulation comparisons at 200 Hz and 5º look fairly good, except the theory slightly overpredicts the spectral energy at lower frequencies. Similar to the 75 Hz case, the slope changes at 0.2 cph, in agreement with the theory. Comparing with the 0º ray at 200 Hz however, we see much less spectral energy for frequencies of variability greater than *N*.

Figure (21) shows the phase spectrum of the theory and simulation at 200 Hz and 10° launch angles at the predefined ranges seen in Table 2. Comparisons for the 10º ray are similar to the 5º ray. Again, the theory overpredicts the spectral energy at low frequencies of variability. We see a clear shift in spectral slope at about 0.5 cph. Spectral energy is also seen to extend to the frequencies of variability greater than *N* at larger ranges.

Figure (22) shows the phase spectrum of the theory and simulation at 200 Hz and 14° launch angles at the predefined ranges seen in Table 2. The 14º ray shows a similar situation to the 75 Hz calculation. The theory underpredicts the spectral energy for frequencies lower than 1 cph and does a relatively good job matching the theory and simulation for the frequencies of variability greater than 1 cph. Here the spectral energy at frequencies of variability greater than N is quite small. So it is clear that energy penetrating into frequencies of variability greater than N seems to diminish with increasing beam angle. This means that interference effects which cause the extension at high frequencies of variability diminish with increasing beam angle.

3. Spectral Energy at 400 Hz

Figure (23) shows the phase spectrum of the theory and simulation at 400 Hz and 0° launch angles at the predefined ranges seen in Table 2. Comparisons are similar to the 75 Hz and 0º case. We observed that the Rytov theory and the simulation results are in good agreement between buoyancy frequency and inertial frequency in which ω^{-3} spectral form is observed. However, the spectral energy at frequencies greater than buoyancy frequency is higher at lower ranges than for the 200 Hz case. We observed that interference effects are significant past the 100 km range, where the ω^{-3} shape continues until the highest frequency of variability of 20 cph. Also, at higher ranges the theory slightly overpredicts the spectral energy at lower frequencies of variability.

Figure (24) shows the phase spectrum of the theory and simulation at 400 Hz and 5° launch angles at the predefined ranges seen in Table 2. The comparisons at 5º look good, except the theory slightly overpredicts the spectral energy at the lowest frequencies of variability. As observed in both the 75 Hz and 200 Hz calculations, the change in slope occurs at 0.2 cph. Comparing with the 400 Hz and 0º calculations, the spectral energy at frequencies of variability higher than buoyancy frequency is much less, except at 200 km where the ω^{-3} form extends up to the highest frequency of variability of 20 cph.

Figure (25) shows the phase spectrum of the theory and simulation at 400 Hz and 10° launch angles at the predefined ranges seen in Table 2. The theory and the simulation are in agreement between the buoyancy frequency and inertial frequency. The theory slightly overpredicts at lower frequencies of variability, and spectral energy extends to

the frequencies of variability greater than *N* at lower ranges than for 200 Hz. Spectral energy for the frequencies of variability greater than *N* is lower than the spectral energy at 5º and much less than the spectral energy at 0º.

Figure (26) shows the phase spectrum of the theory and simulation at 400 Hz and 14° launch angles at the predefined ranges seen in Table 2. The comparisons for 400 Hz and 14° beam are very similar to the earlier comparisons for 14º at 75 Hz and 200 Hz. The theory significantly underpredicts the spectral energy for the frequencies of variability lower than 1 cph, and it works well after 1 cph. Also, energy penetrating into the region where frequencies of variability are greater than *N* is much less than that at lower beam angles.

D. LOG-AMPLITUDE SPECTRA

In this section we will analyze the frequency spectrum of log-amplitude. As before, the analysis is made for 12 cases, with 3 different frequencies of 75, 200, and 400 Hz, and for each frequency 4 different launch angles of 0°, 5°, 10° , and 14°. Analysis results are plotted for 12 cases starting from Figure (27) for 75 Hz and 0° launch angle and ending with Figure (38) for 400 Hz and 14° angle.

The red curves are the spectra of phase S_χ from the simulation, and the blue curves are spectra of log-amplitude from the theory. The green curve is the spectrum of μ from the internal wave simulation. In this section we will compare the theoretical results with the simulation for log-amplitude spectra. Each figure has the theoretical value for log-amplitude variance in the title. Ranges used for different launch angles in each subplot are given in Table 2.

1. Spectral Energy at 75 Hz

Figure (27) shows the log-amplitude spectrum of the theory and the simulation at 75 Hz and 0° launch angles. For log-amplitude at 75 Hz and 0° launch angles, the theory overpredicts for frequencies less than 0.2 cph. At the higher frequencies where the ω^{-3} form is observed, the theory predicts very well. For frequencies greater than buoyancy frequency, the theory and the simulation are in agreement.

Figure (28) shows the log-amplitude spectrum of the theory and the simulation at 75 Hz and 5° launch angles. For the log-amplitude at 75 Hz and 5° beam at lower frequencies of variability (ω<0.2 cph), the theory overpredicts. We observe the slope change at 0.2 cph in agreement with the theory. For ω>N the theory is still in agreement with the simulation.

Figure (29) shows the log-amplitude spectrum of the theory and the simulation at 75 Hz and 10° launch angles. The theory works very well at 75 Hz and 10º launch angles. As a result of being a much steeper ray, the change in the spectrum slope occurs at 0.5 cph. Importantly, the slope before the cutoff frequency is in agreement between the theory and the simulation. In general, the shape of the spectra is excellent.

Figure (30) shows the log-amplitude spectrum of the theory and the simulation at 75 Hz and 14° launch angles. For the log-amplitude prediction at 75 Hz and 14° beam, the theory breaks down for the frequencies of variability lower than 1 cph. The theory significantly underpredicts the spectral energy for the frequencies lower than 1 cph. However, the theory is relatively accurate at higher frequencies of variability where the spectral slope very nearly has the ω^{-3} shape. At 75 Hz we do not observe high spectral energy for frequencies greater than the buoyancy frequency (ω>N).

2. Spectral Energy at 200 Hz

Figure (31) shows the log-amplitude spectrum of the theory and the simulation at 200 Hz and 0° launch angles. In general, the theory slightly overpredicts at lower frequencies of variability. At the 100 km range, the ω^{-3} spectral slope form extends up to the highest frequency of variability, past the buoyancy frequency. Past the 100 km range, the theory does not predict the energy at frequencies greater than buoyancy frequency.

Figure (32) shows the log-amplitude spectrum of the theory and the simulation at 200 Hz and 5° launch angles. At 106 km, the theory predicts the log-amplitude very well at frequencies of variability greater than 0.2 cph, while it still slightly overpredicts the spectral energy at lower frequencies of variability. At longer ranges the theory is not good at very low and high frequencies. We observe a slope change at 0.2 cph in agreement with the theory. At longer ranges the simulation shows spectral energy

extending to the highest frequency of variability of 20 cph. We observed spectral energy where $\omega > N$ at longer ranges. Importantly, at 200 km the spectral slope is slightly flattened, so it does not quite show the ω^{-3} form.

Figure (33) shows the log-amplitude spectrum of the theory and the simulation at 200 Hz and 10° launch angles. The theory slightly overpredicts for the 68 km range and $\omega < 0.5$ cph. At higher ranges the theory slightly overpredicts below 0.1 cph, and the theory slightly underpredicts after 0.1 cph. We do not observe the ω^{-3} form above 0.5 cph; instead we observe the flattening of the spectral slope due to the effects of ω_L. At higher ranges the ω^{-3} form extends up to the highest frequency of variability of 20 cph.

Figure (34) shows the log-amplitude spectrum of the theory and the simulation at 200 Hz and 14° launch angles. As in all the other cases for 14º, the theory breaks down for frequencies lower than 1 cph, where the theory dramatically underpredicts the spectral energy. For frequencies greater than 1 cph, the theory works well and the spectral energy at higher frequencies of variability observed at the lower beams is diminished.

3. Spectral Energy at 400 Hz

Figure (35) shows the log-amplitude spectrum of the theory and the simulation at 400 Hz and 0° launch angles. At 400 Hz and 0° launch angles, the theory slightly overpredicts for frequencies of variability lower than 0.2 cph. For frequencies of variability greater than 0.2 cph at low ranges the theory works well. Also, the theory does not predict the spectral energy at higher frequencies of variability, whereas the simulation results are extended up to the highest frequency of variability.

Figure (36) shows the log-amplitude spectrum of the theory and the simulation at 400 Hz and 5° launch angles. For the 400 Hz and 5° beam, the theory slightly overpredicts at frequencies of variability lower than 0.2 cph. For frequencies of variability greater than 0.2 cph, the spectral slope changes and takes the ω^{-3} form where the results are much better than lower frequencies of variability and the 400 Hz 0º beam. The theory does not predict the spectral energy at higher frequencies than the buoyancy frequency, whereas the simulation results show spectral energy up to the highest frequency of variability of 20 cph.

Figure (37) shows the log-amplitude spectrum of the theory and the simulation at 400 Hz and 10° launch angles. For the 400 Hz and 10° beams, the theory works very well between the buoyancy frequency and inertial frequency. The theory underpredicts the spectral energy at lower frequencies. Both the theory and the simulation show a change in spectral slope at 0.5 cph. For frequencies of variability greater than 0.2 cph the slope is nearly ω^{-3} where the theory and the simulation are in agreement. At 200 km the spectral slope form of ω^{-3} continues until the highest frequency of variability of 20 cph.

Figure (38) shows the log-amplitude spectrum of the theory and the simulation at 400 Hz and 14° launch angles. For 400 Hz and 14° launch angles, the theory breaks down for frequencies lower than 1 cph, where the theory significantly underpredicts the spectral energy. At frequencies greater than 1 cph, the theory is working relatively accurately. The spectral energy at higher frequencies of variability past the buoyancy frequency, observed at the lower beams, is diminished for the 14º beam.

E. SUMMARY

In this chapter we analyzed the phase variance, intensity variance, phase spectra, and the intensity spectra for 0º, 5º, 10º and 14º beams and the acoustic frequencies of 75, 200, and 400 Hz. The analysis results are given in Figure (13) through Figure (38).

1. Spectral Comparisons for $f < \omega < 0.2\text{-}1.0$ cph

For the internal wave frequencies between the Coriolis frequency f and the transient frequencies of 0.2-1.0 cph, the Rytov resonance with perpendicular internal wave (IW) wave numbers limits the influence of low-frequency internal waves. In this low frequency of variability regime, the Rytov theory results are in good agreement with the simulations for the grazing angles between 0º and 10º. However, at the 14º grazing angle, the Rytov theory dramatically underpredicts the spectral energy, demonstrating a breakdown in the Rytov resonance condition.

2. Spectral Comparisons for 0.2-1.0cph$< \omega <N$

For the frequencies of variability between the transient frequency and the buoyancy frequency N, the Rytov theory and the Monte Carlo numerical simulation spectra are in very good agreement at all acoustic frequencies and beam grazing angles.

In this frequency region the slope of the spectra is nearly -3. However, the spectral slope of log-amplitude is slightly weakened at the longer ranges and higher acoustic frequencies.

3. Spectral Comparisons for $\omega > N$

When there is significant variability in phase and log-amplitude, significant spectral energy can exist at frequencies greater than the buoyancy frequency (the maximum internal wave frequency). This energy is not predicted by the Rytov model and represents the effect of strong interference and scattering not treated in the weak fluctuation approach of the Rytov theory.

THIS PAGE INTENTIONALLY LEFT BLANK

VI. CONCLUSIONS AND FUTURE WORK

The objective of this thesis was to examine efficient reduced physics models for estimating acoustic propagation through the fluctuating ocean. This research is a study to predict acoustic propagation statistics using "simple" analytic models rather than doing intensive and time-consuming Monte Carlo computations.

The primary research focus of this thesis was the establishment of the regimes of validity of the Rytov theory. This addresses the important problem of characterizing the acoustic uncertainty in the ocean sound channel. The acoustic observable of the frequency spectrum of phase and log-amplitude was used for this analysis, since many other acoustic observables, namely amplitude and phase correlation functions and coherence, can be directly derived from these spectra. Using Monte Carlo numerical simulation methods utilizing canonical models of sound speed, buoyancy frequency, and internal wave spectra, this analysis established the acoustic propagation range and acoustic frequency limitations of the Rytov theory, as a function of ray path geometry.

Monte Carlo numerical simulations of acoustic propagation through random fields of internal waves were carried out at acoustic frequencies of 75, 200, and 400 Hz, and the range evolutions of four acoustic ray paths were studied to a maximum range of 200 km.

Ray paths corresponding to grazing angles of 0°, 5°, 10° , and 14° were considered, thus spanning the range of possible ray geometry from surface reflection to axial propagation. At a series of different ranges from the source, frequency spectra were computed and compared to the Rytov theory to establish regimes of validity and the mechanism by which the theory breaks down.

A. CONCLUSIONS

For all acoustic frequencies and beam grazing angles, we observed that the spectral slopes from the Rytov theory and the Monte Carlo numerical simulation are in very good agreement in the frequency range from the buoyancy frequency up to a grazing-angle-dependent transition frequency between 0.2 and 1 cph. In this frequency

range the slope of the spectra is nearly -3. However, the spectra of log-amplitude at the longer ranges and higher acoustic frequencies show some weakening of the -3 slope. The theory breakdown point seems different for these two observables.

For frequencies less than the transition frequency, where the Rytov resonance with perpendicular (internal wave) IW wave numbers limits the influence of low-frequency internal waves, the Rytov theory spectra are in fairly good agreement with the simulations for all ranges and grazing angles between 0º and 10º. For the 14º beam in which there is surface interaction, the Rytov theory dramatically underpredicts the spectral energy at frequencies less than 1 cph, demonstrating a breakdown in the Rytov resonance condition.

For high frequencies of variability in phase and log-amplitude, we also find that significant spectral energy can exist at frequencies greater than the buoyancy frequency. The Rytov theory does not predict this energy. This breakdown represents the effect of strong interference and scattering not treated in the weak fluctuation approach of the Rytov theory.

These results establish the validity regimes of Rytov theory, and show the regions in which we can save time and memory to predict the phase and intensity variations or spectral energy of phase and log-amplitude.

B. RECOMMENDATIONS FOR FUTURE WORK

Further study should be done to validate these simulation results with ocean experiments. As an example, there is an upcoming experiment which will be conducted in the Philippines Sea in 2009. This experiment will use 75 Hz and 250 Hz as their transmission frequencies. Following these simulations and the ocean experiments, the theory breakpoints and the influences behind them should be analyzed. At higher acoustic frequencies in the kHz region, phase spectra results are much better than the intensity spectra results. This study showed that the Rytov theory and simulation results are very close to each other at lower acoustic frequencies. The reasons for better phase spectra results at higher acoustic frequencies should be investigated. Another study should be

undertaken to calculate the coherence function. This phase coherence information could be used to design useful systems, such as the sonar array algorithms, to predict long-range and low-frequency signals.

This study showed the regions where the Rytov theory works well for the maximum frequency or range limit used in this study. Further study should be extended to higher acoustic frequencies and longer ranges to determine the breakdown point at these regions. In the future, work should be done to understand the physics behind the strong interference and scattering at frequencies of variability greater than the buoyancy frequency. This thesis study showed that the theory worked well at 10 º grazing angles, but it broke down at 14º. Further study should be done to analyze the grazing angles between 10º and 14º to find a more accurate breakdown point.

The spectrum information can be used in the signal processing algorithms to improve the signal to noise ratio (SNR) for underwater communication systems. This thesis study used the Munk's canonical sound-speed profile in the Monte Carlo numerical simulation. The sound-speed field could have a much more complex profile than this study used, and testing should be repeated for these sound-speed profiles.

THIS PAGE INTENTIONALLY LEFT BLANK

APPENDIX. FIGURES

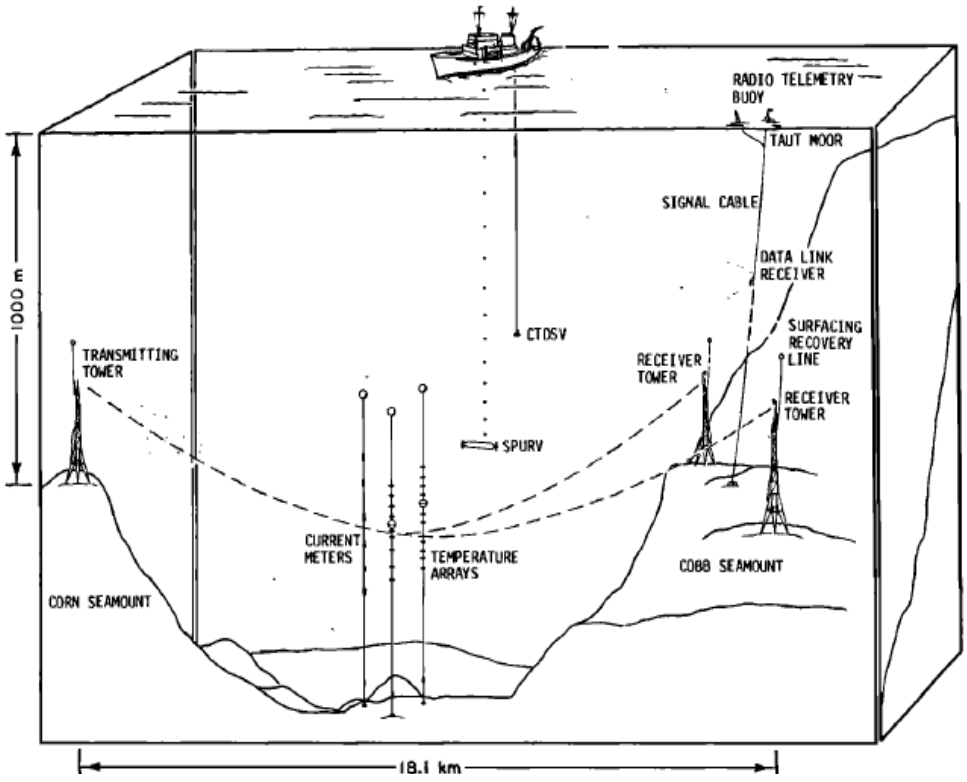

Figure 1. Diagrammatic overview of MATE (From: Ewart and Reynolds, 1984).

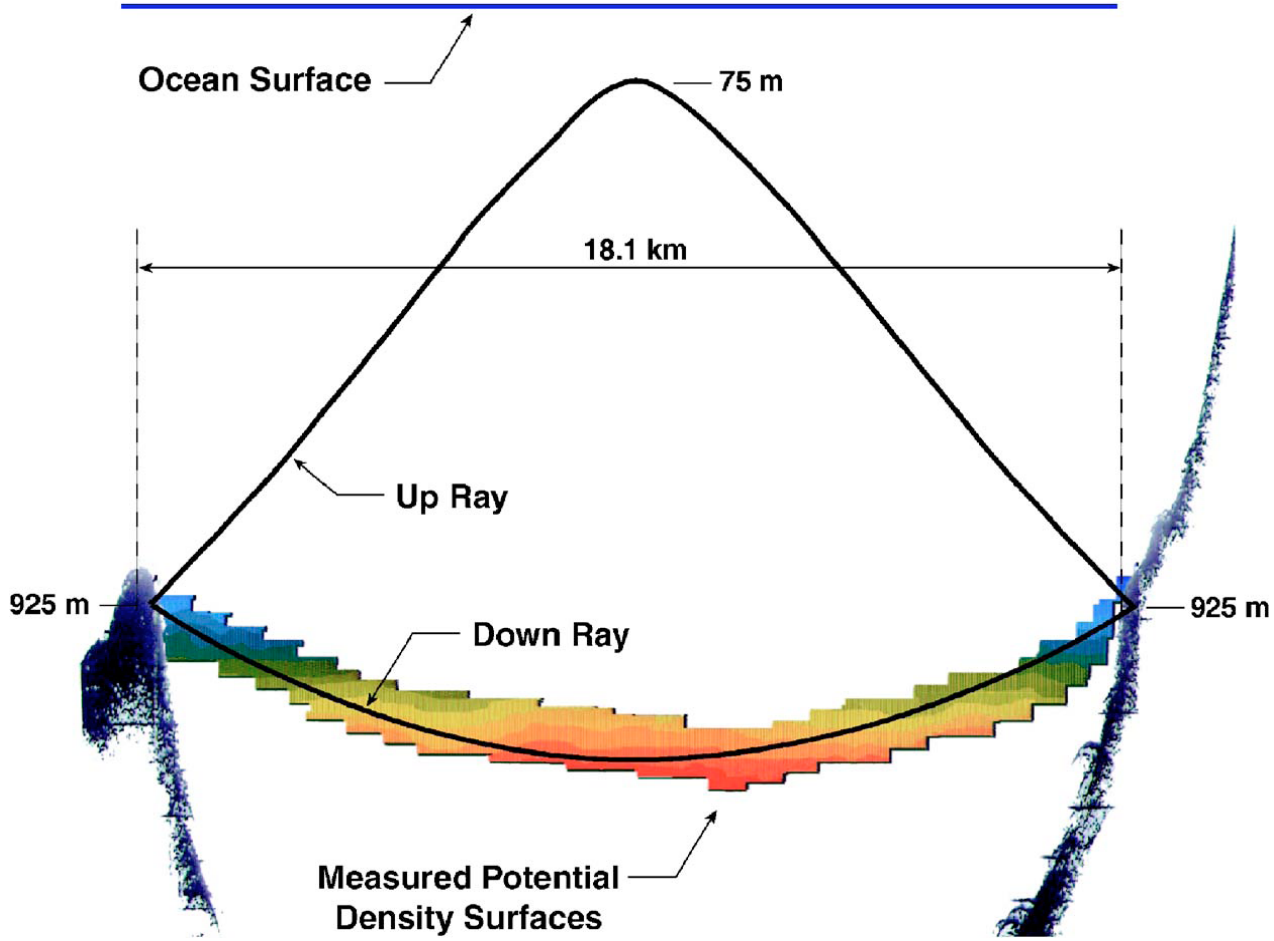

Figure 2. (Color online) Local bathymetry from the precision depth recorder, upper path and lower path eigen rays traced using the mean sound speed profile, and potential density contours taken with an autonomous vehicle, SPURV, depth cycling over the lower ray. The gray scale are equally spaced, with a total range of 0.2 Kg/ m^3 . (From: Henvey and Ewart, 2006).

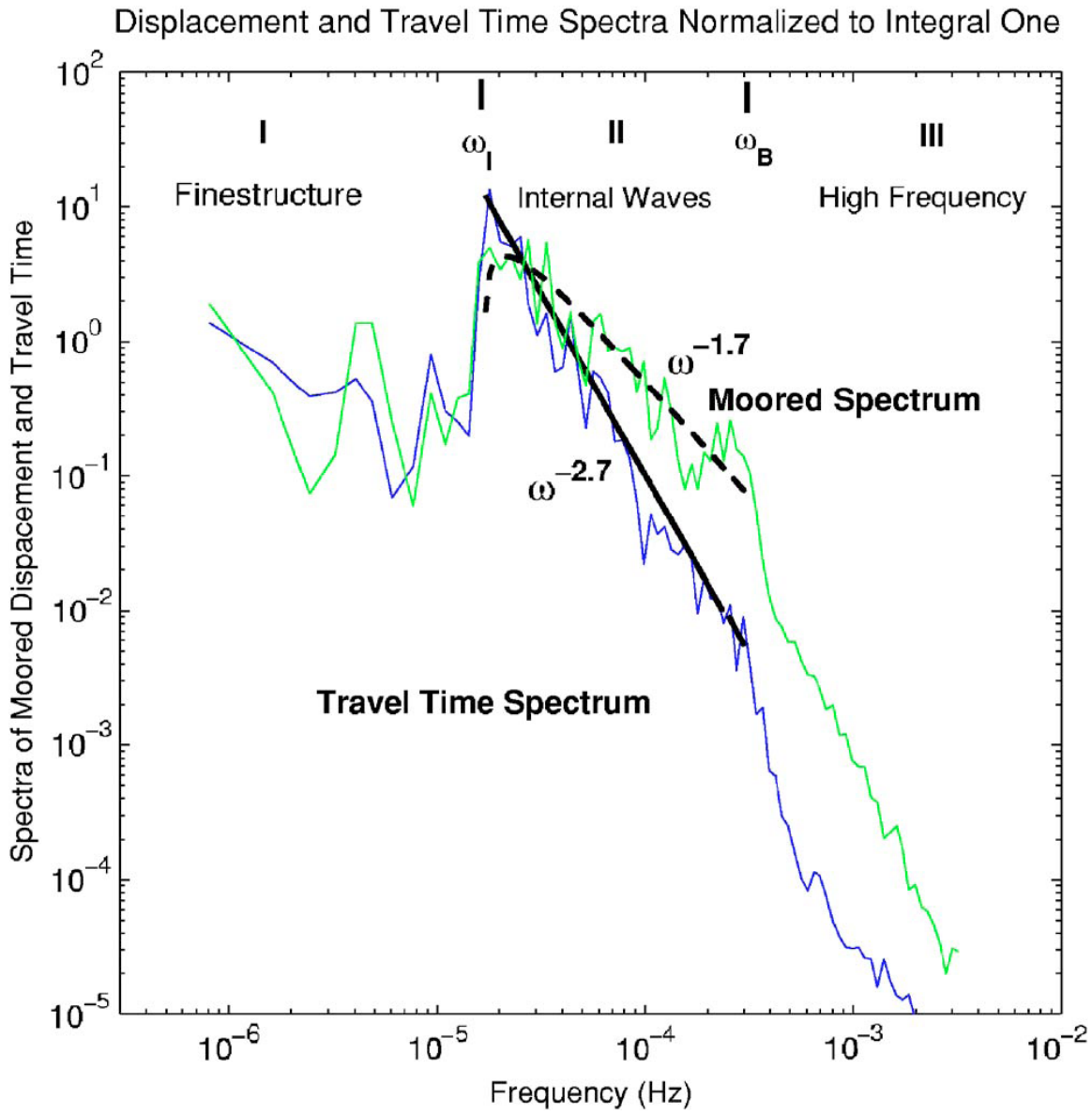

Figure 3. (Color online) Spectra of the moored displacement and travel time measured during MATE (normalized to integral one). The fit of the model to the moored spectrum and its prediction for the travel time spectrum are shown. (From: Frank and Terry E. Ewart, 2006).

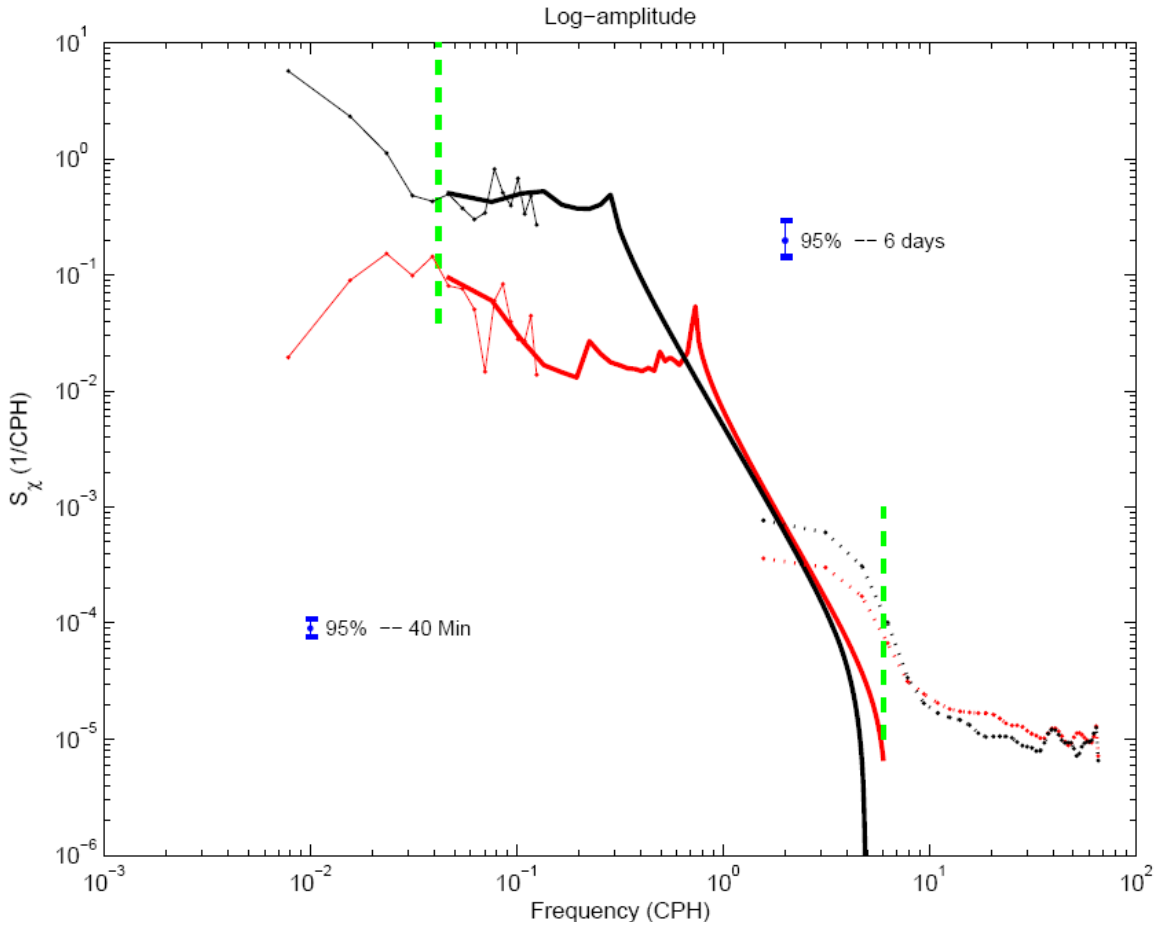

Figure 4. AET frequency spectrum of log-amplitude. The red curve is a ray angle of 10°, and the black curve is a ray angle of 5°. The solid curves are the theory. (From: Colosi and Xu , 2007).

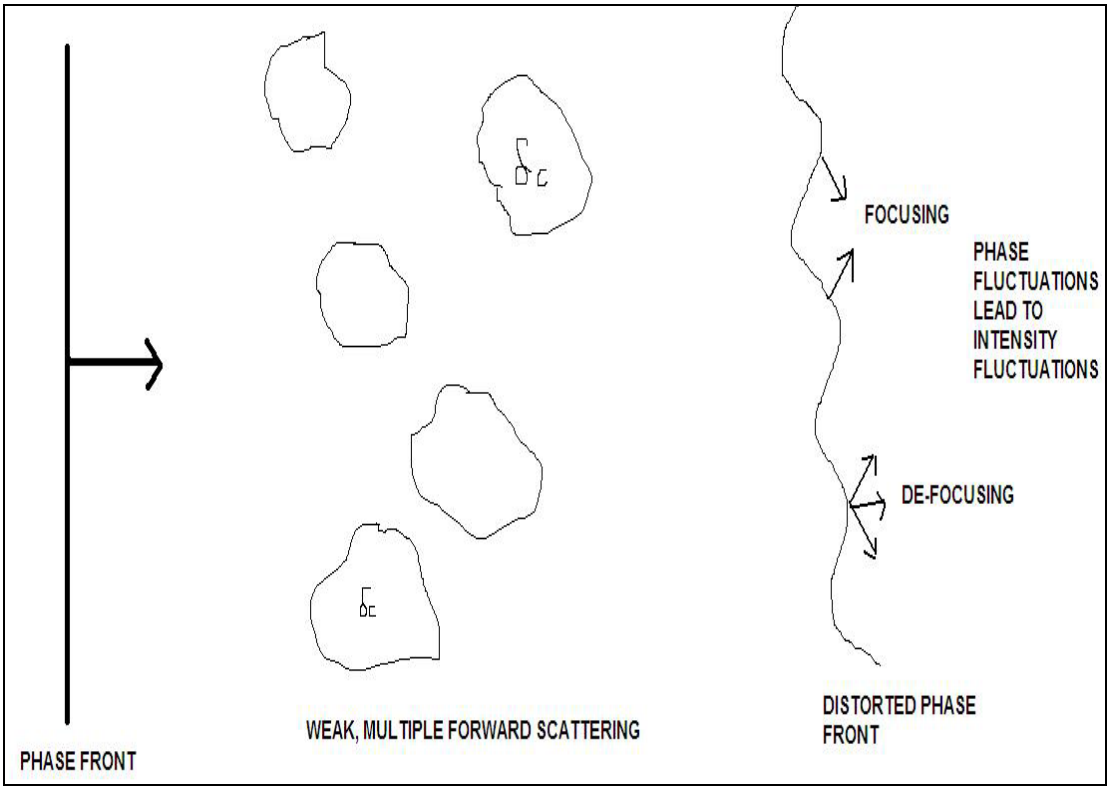

Figure 5. Weak, multiple forward scattering.

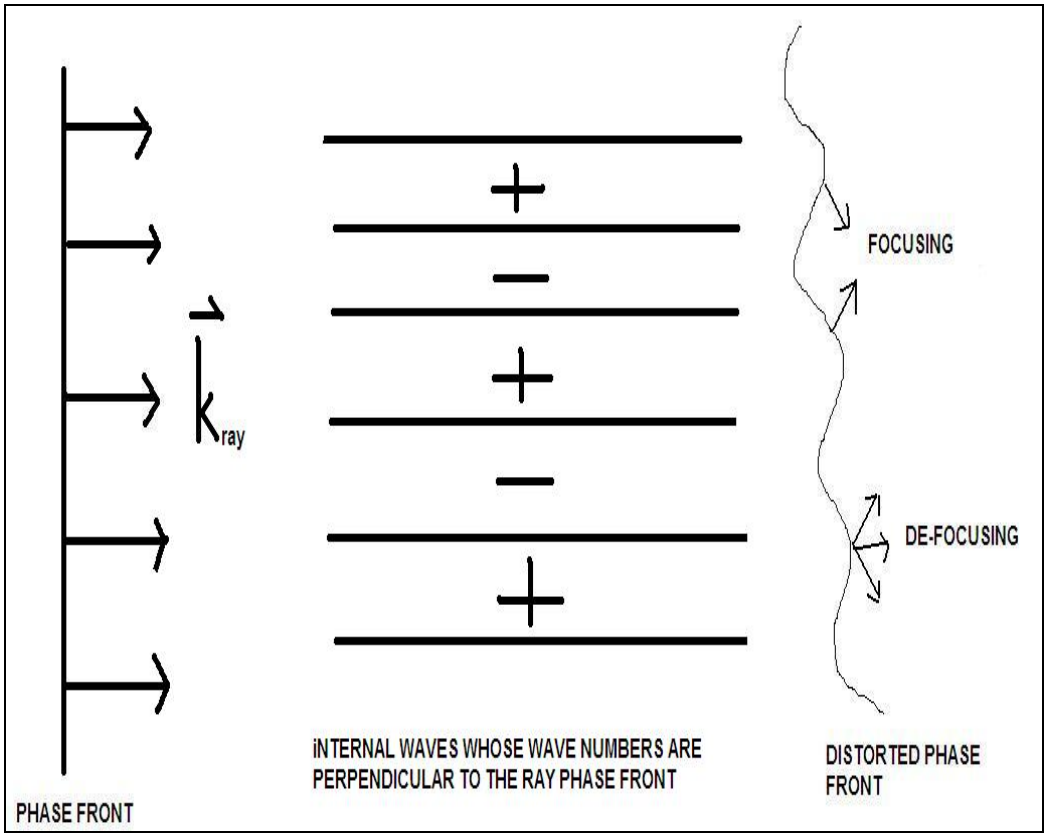

Figure 6. Internal waves whose wave numbers are perpendicular to the ray contribute to the scattering. + shows higher speed and - shows lower speed.

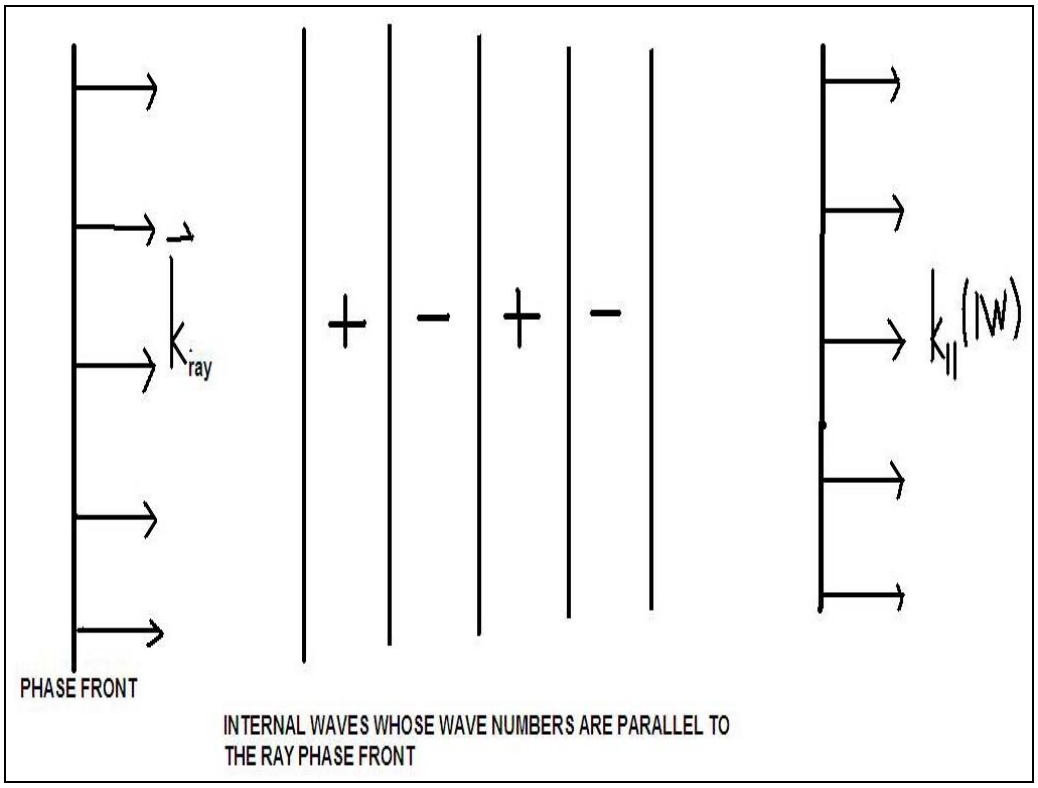

Figure 7. Internal waves whose wave numbers are parallel to ray phase front do not contribute to the scattering.

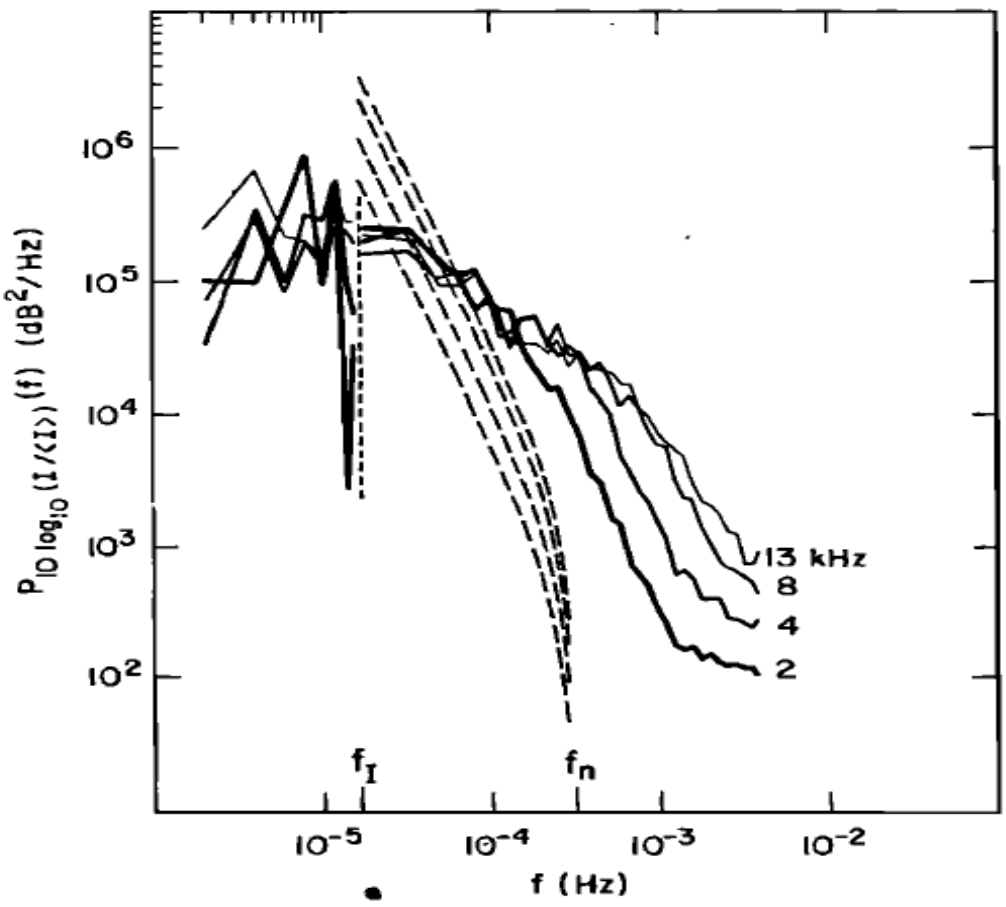

Figure 8. Spectra of Log-Amplitude taken from MATE experiment (From: Ewart, Reynolds, 1984).

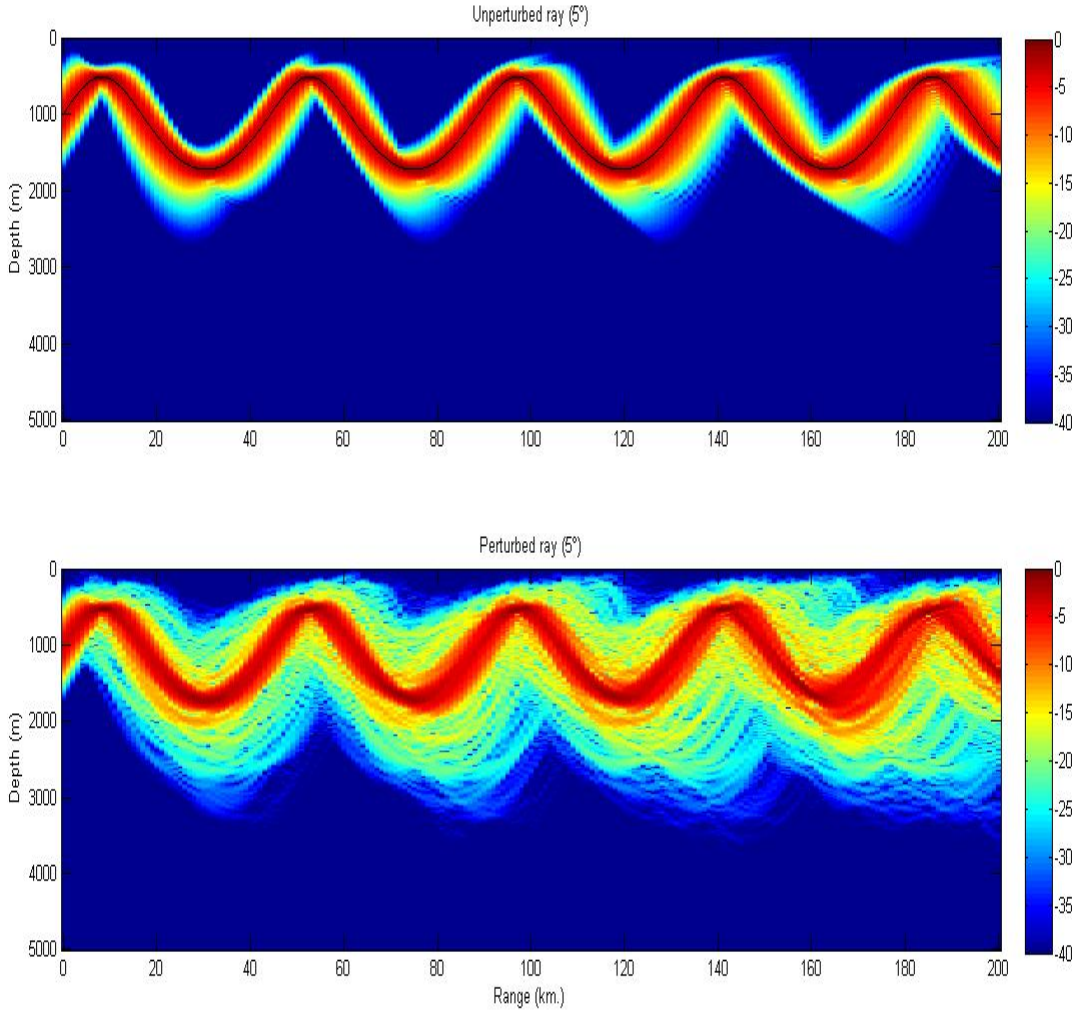

Figure 9. Sound propagation at 200 Hz and 5° launch angle (a)Unperturbed ray and (b) Perturbed ray.

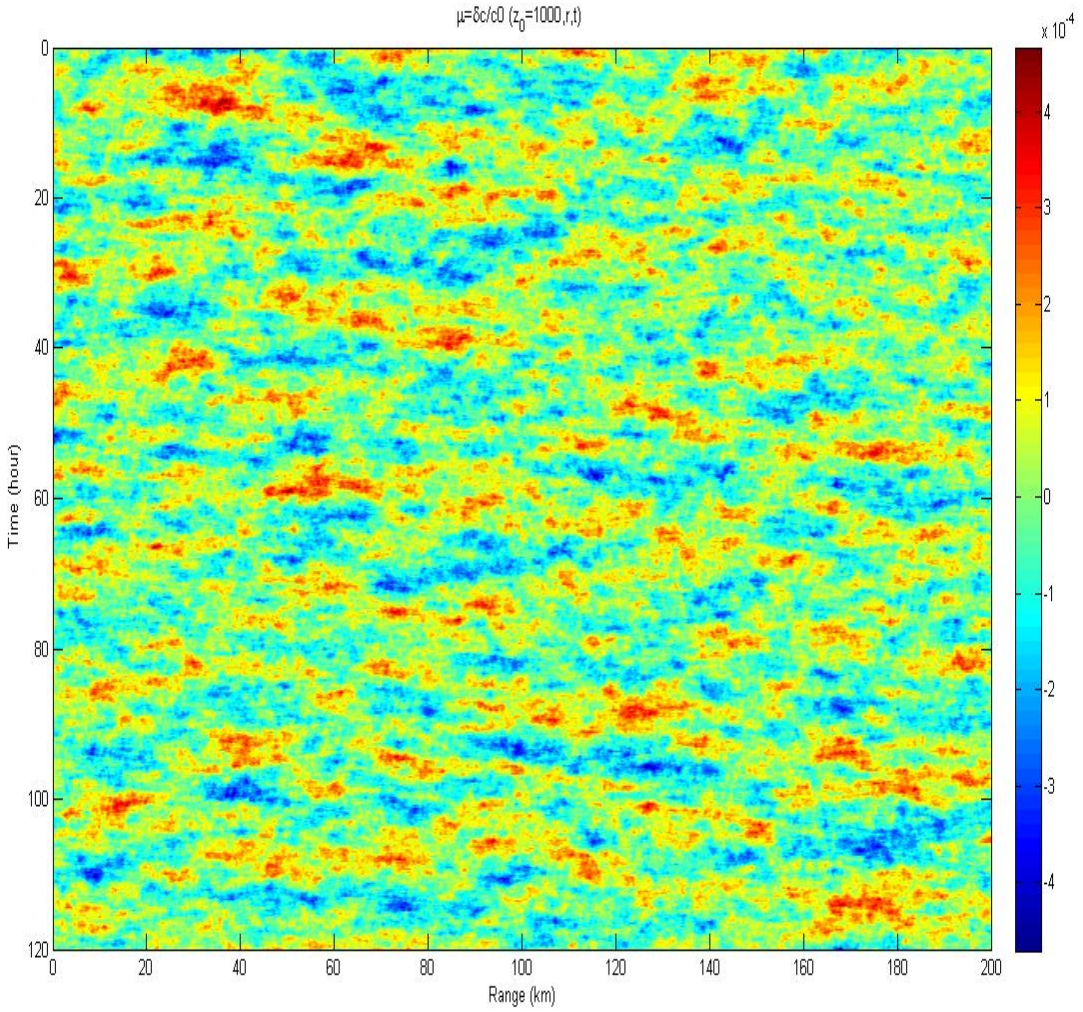

Figure 10. Sound speed fluctuation from the deterministic sound channel ($\frac{\delta c}{c_0}(z_0 = 1000m., r, t)$).

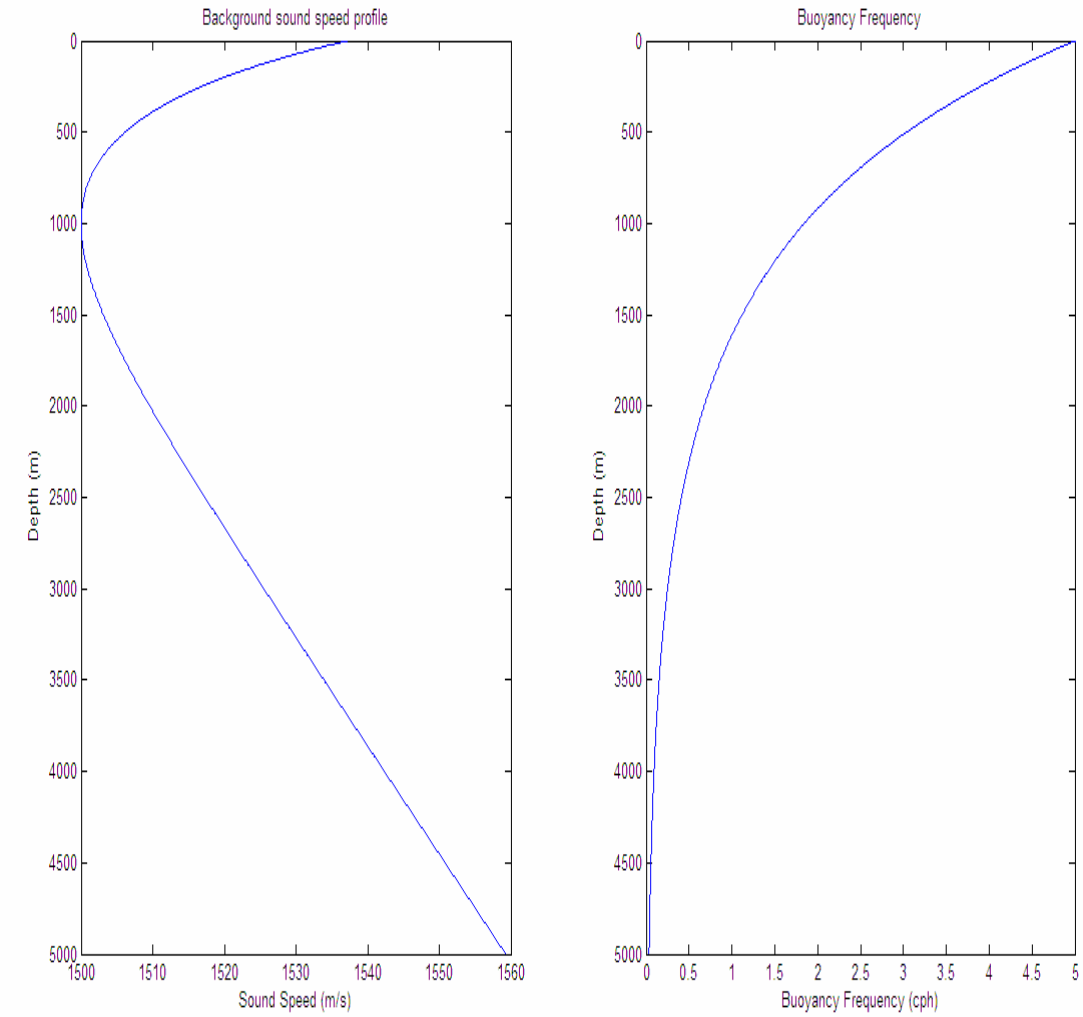

Figure 11. Background sound speed profile and buoyancy frequency profile used in the simulation.

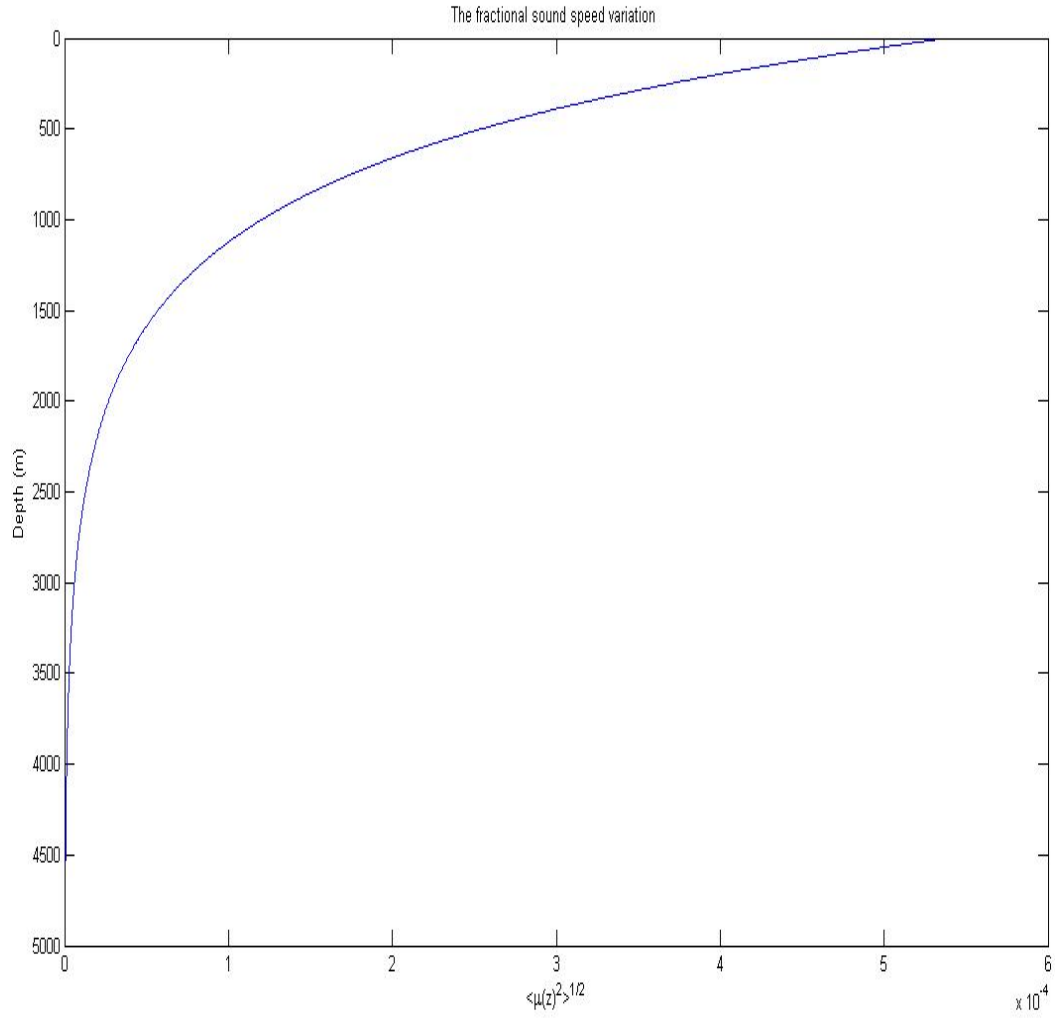

Figure 12. The fractional sound speed variation $\left\langle \mu^2(z) \right\rangle^{1/2}$.

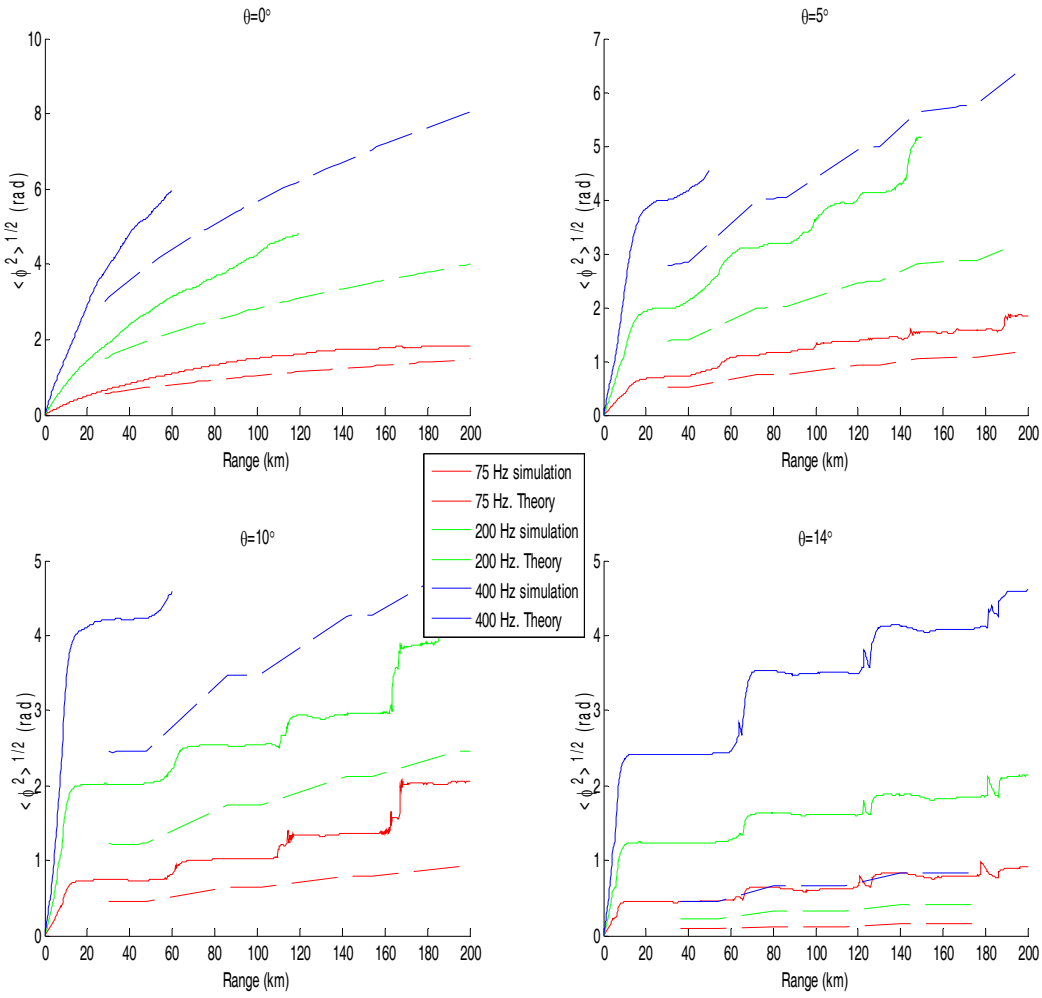

Figure 13. The rms value of phase variance $\left\langle \phi^2 \right\rangle^{1/2}$ (rad).

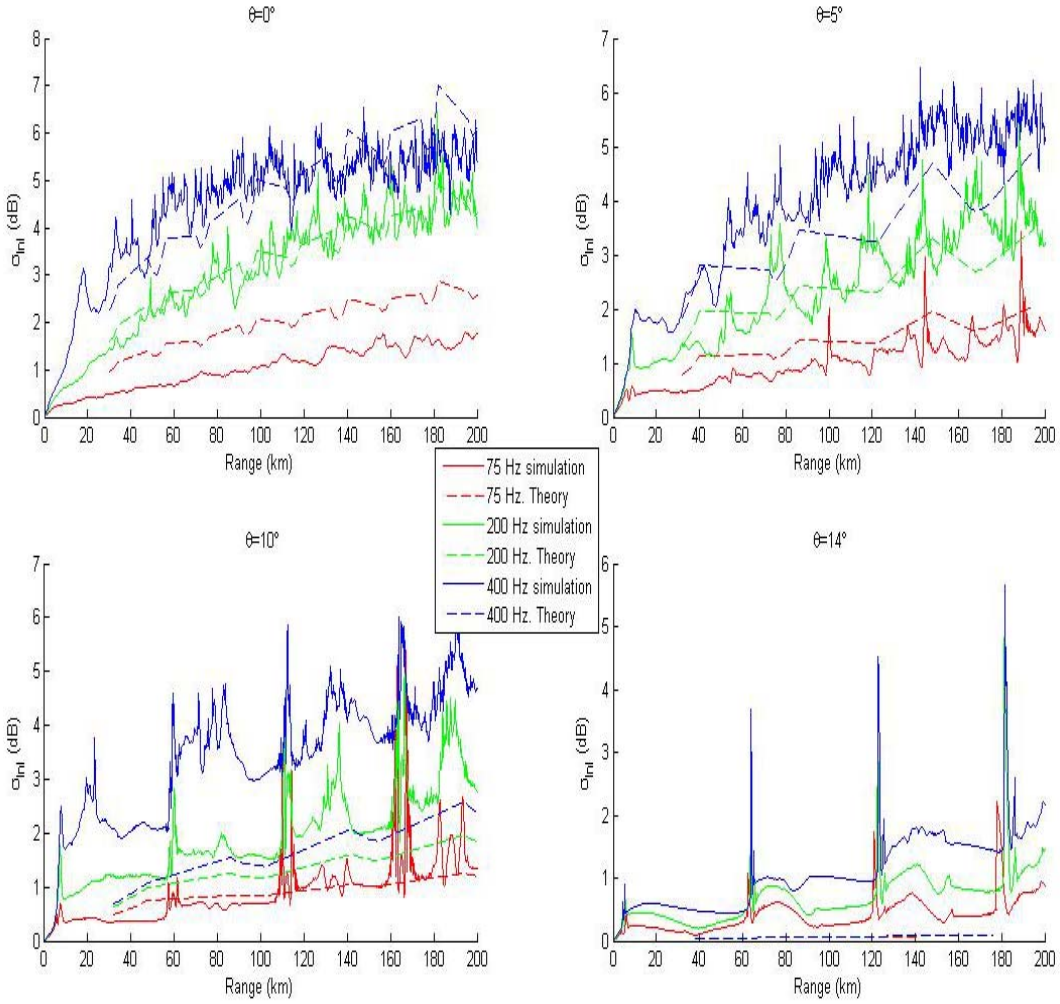

Figure 14. Intensity fluctuations.

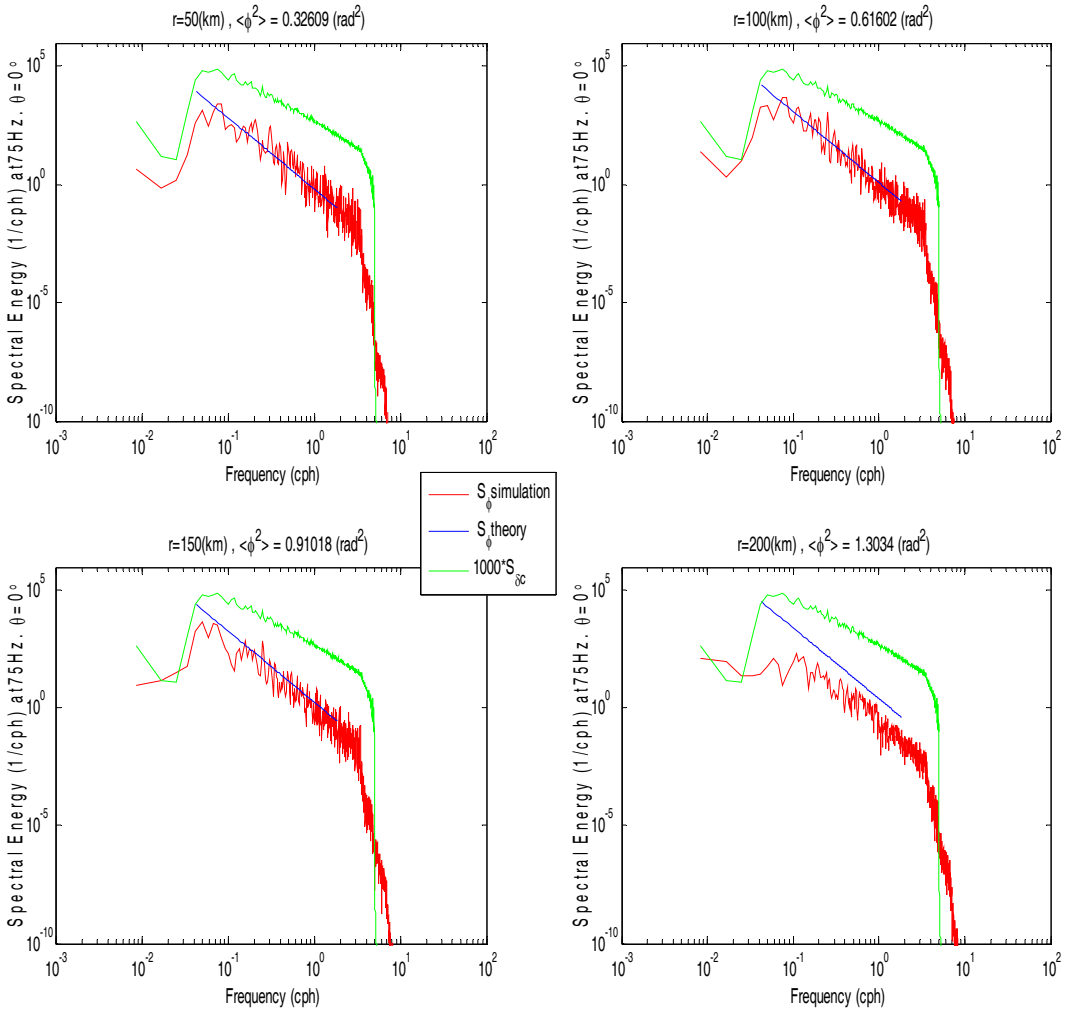

Figure 15. Phase spectra at 75 Hz and $\theta = 0°$ {Simulation results are plotted with red and theory is plotted with blue, μ spectra is plotted with green}.

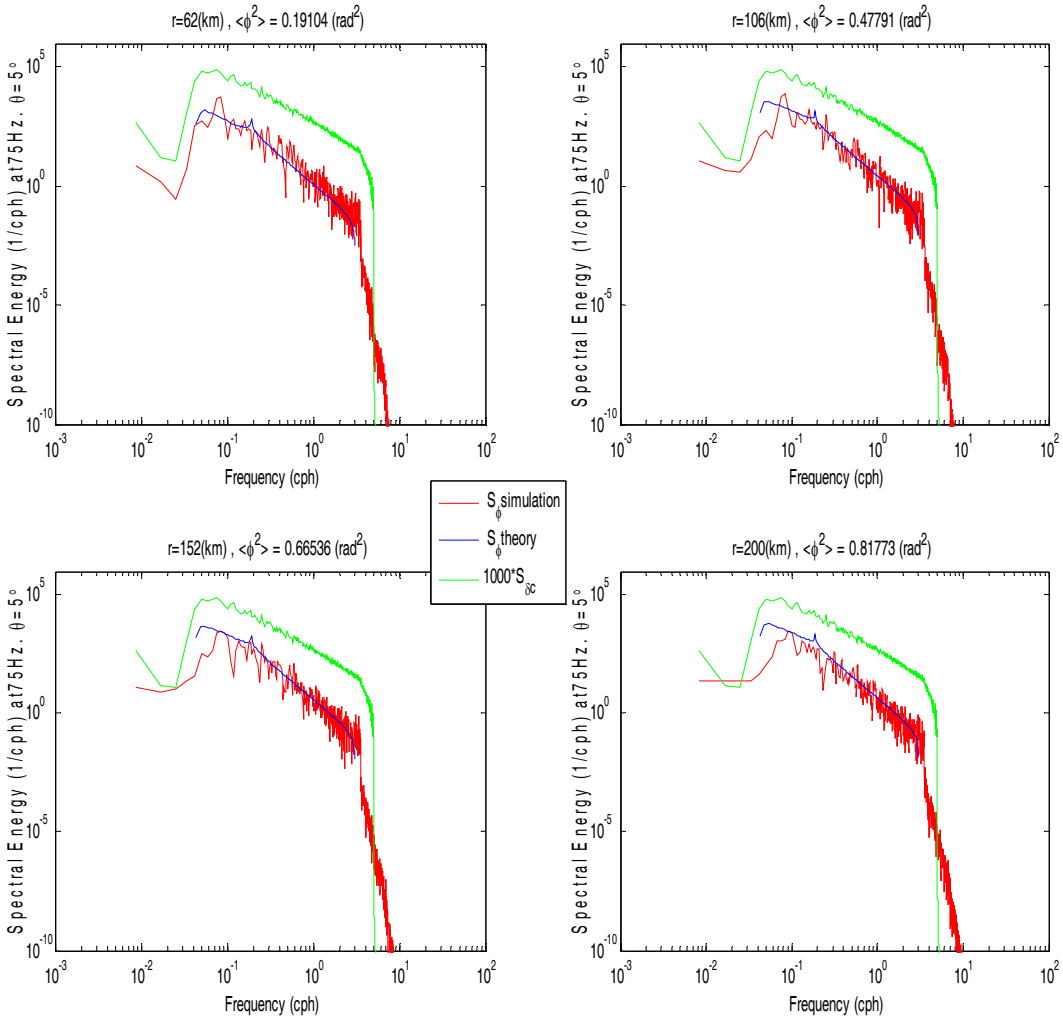

Figure 16. Phase spectra at 75 Hz and $\theta = 5°$.

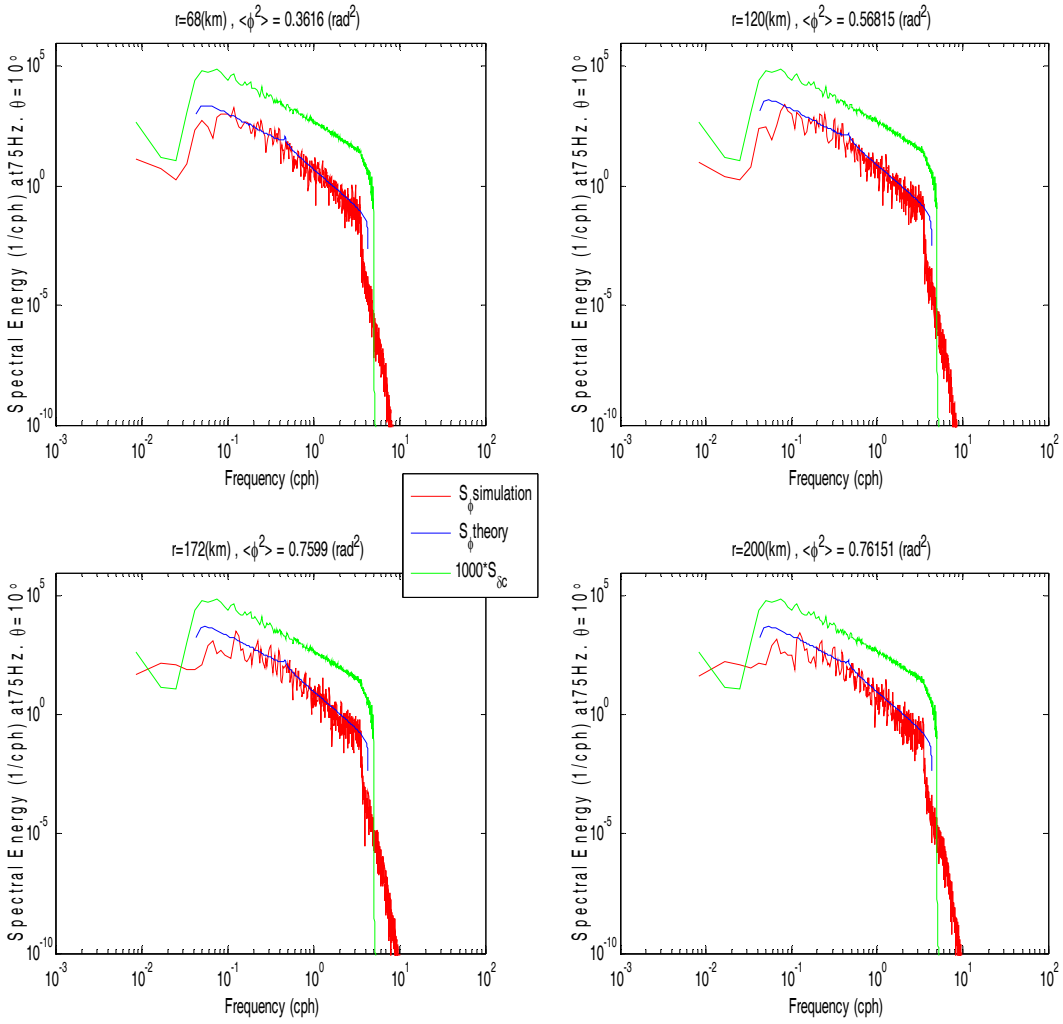

Figure 17. Phase spectra at 75 Hz and $\theta = 10°$.

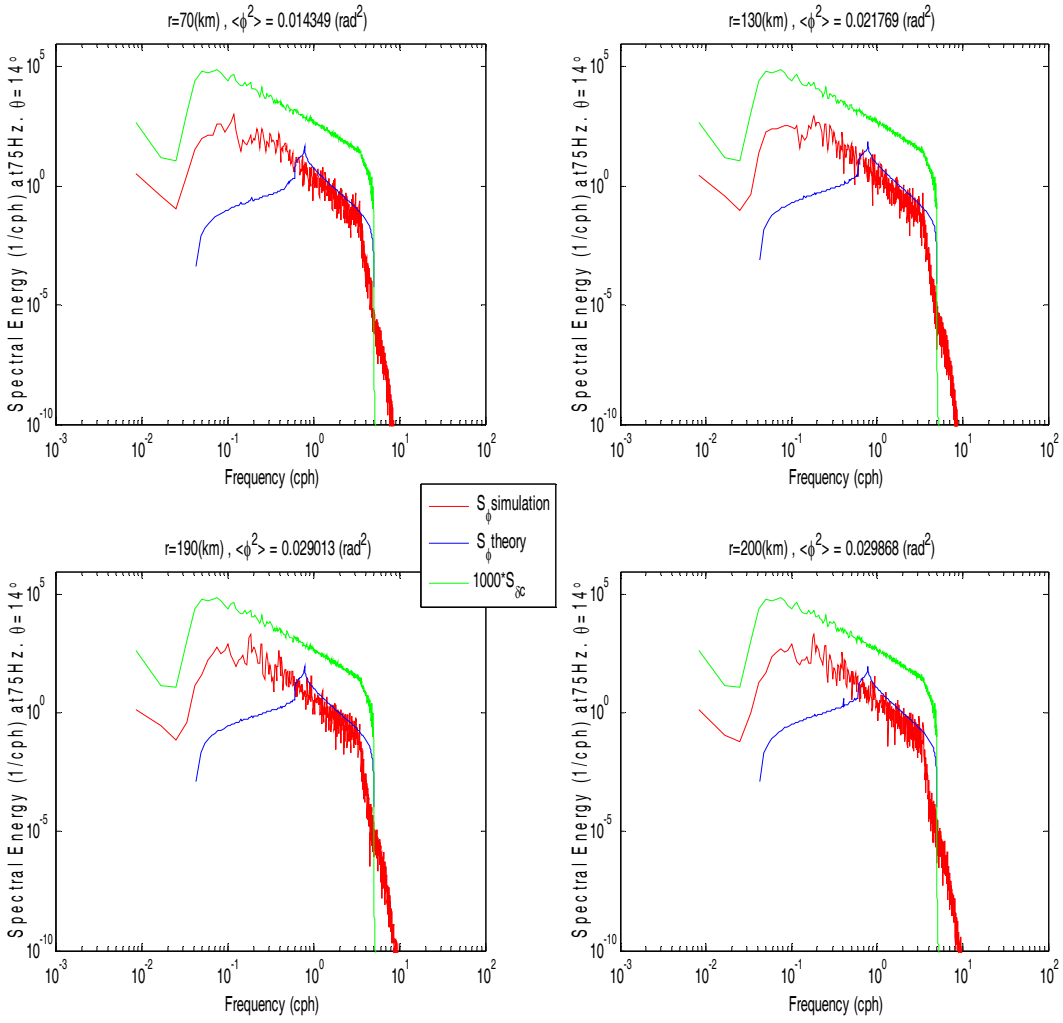

Figure 18. Phase spectra at 75 Hz and $\theta = 14°$.

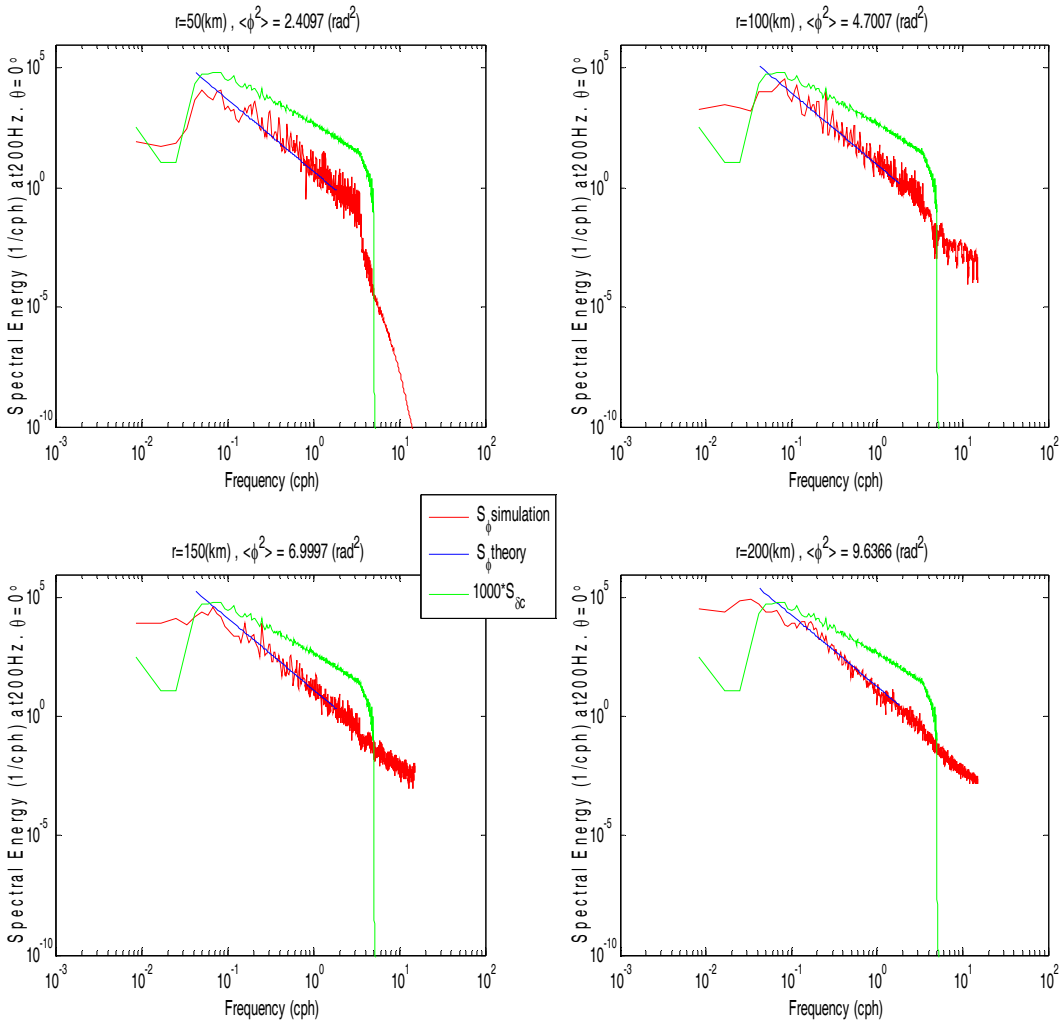

Figure 19. Phase spectra at 200 Hz and $\theta = 0°$.

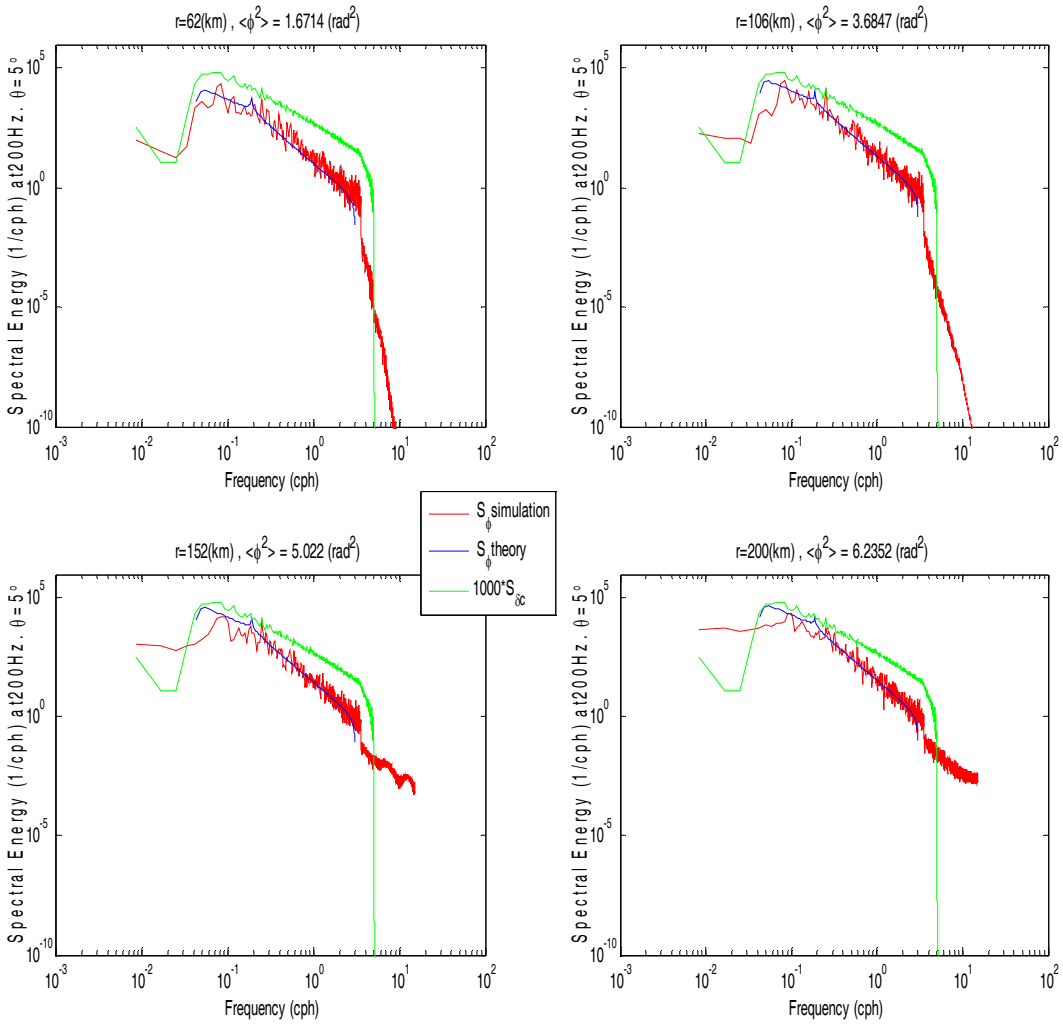

Figure 20. Phase spectra at 200 Hz and $\theta = 5°$.

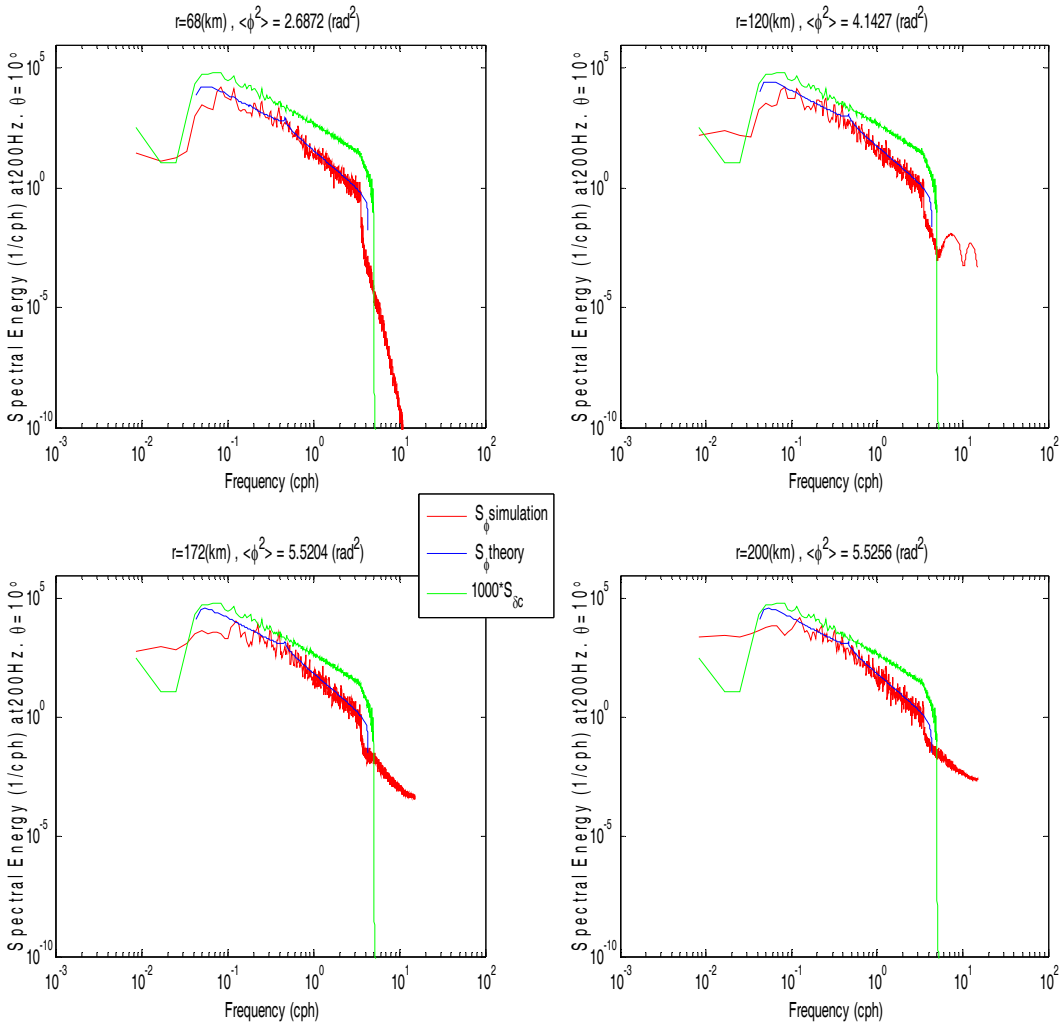

Figure 21. Phase spectra at 200 Hz and $\theta = 10°$.

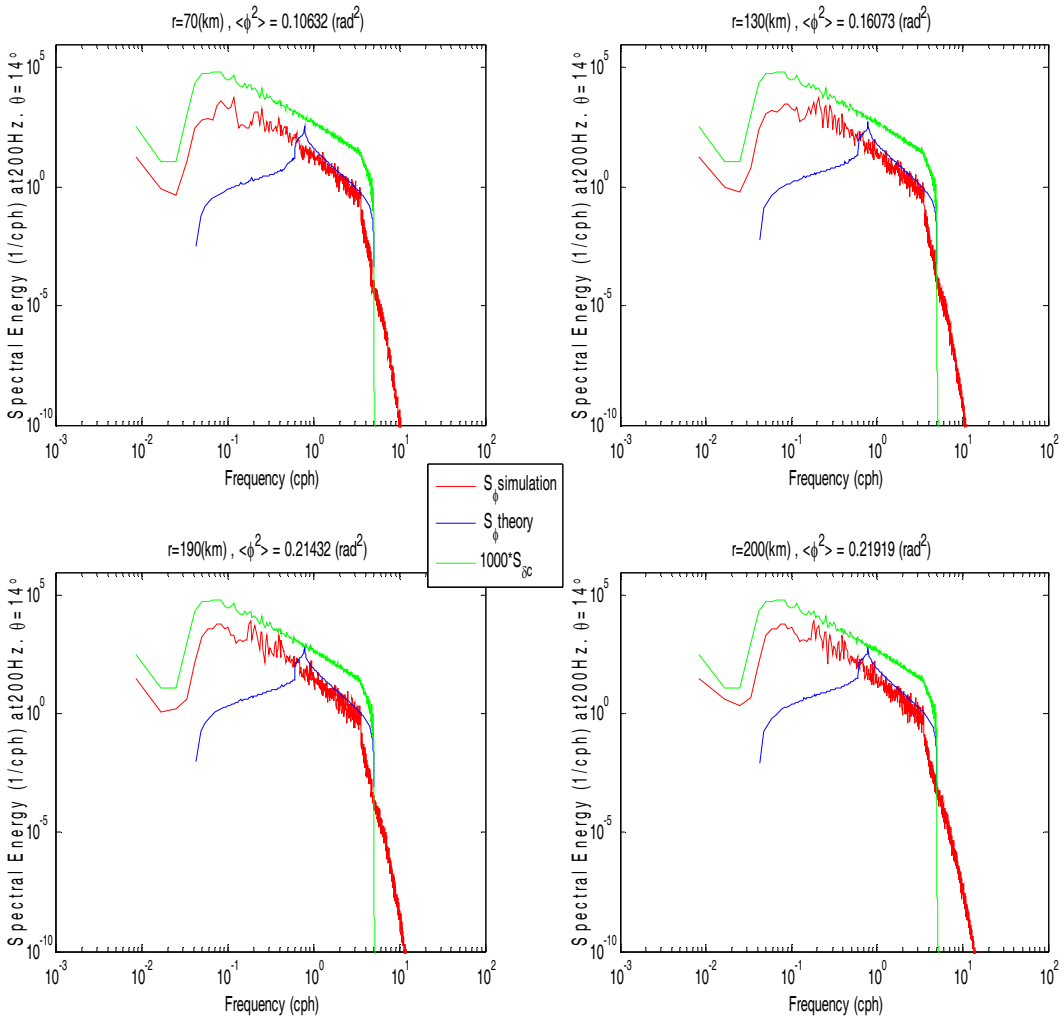

Figure 22. Phase spectra at 200 Hz and $\theta = 14°$.

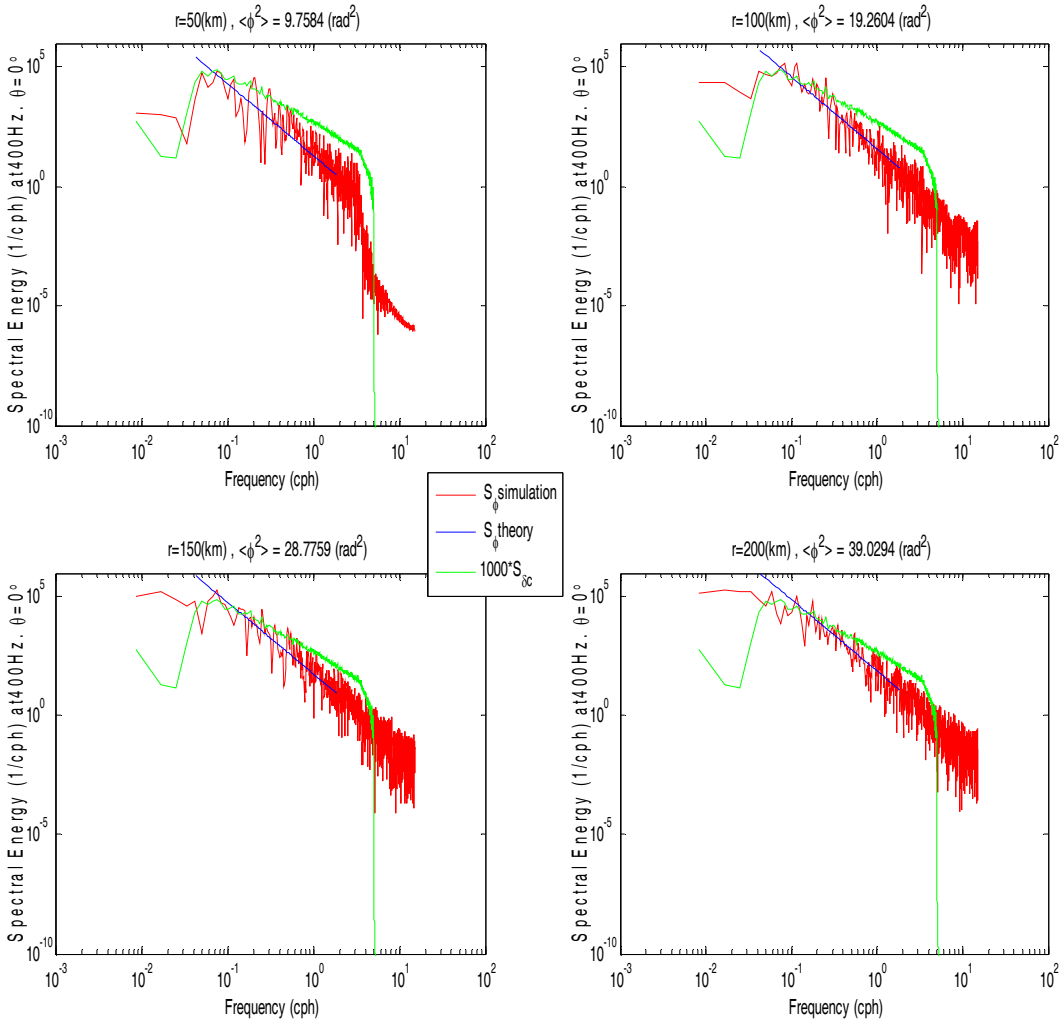

Figure 23. Phase spectra at 400 Hz and $\theta = 0°$.

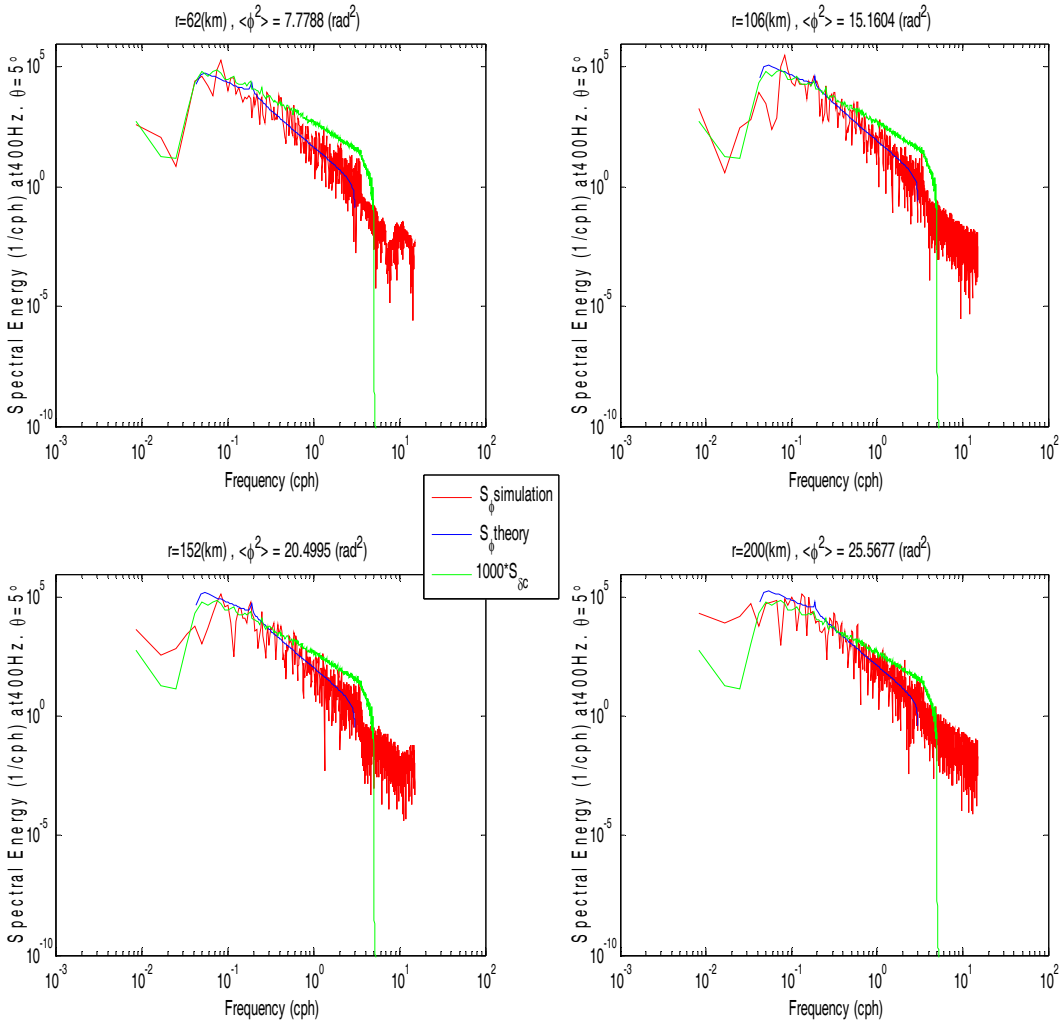

Figure 24. Phase spectra at 400 Hz and $\theta = 5°$.

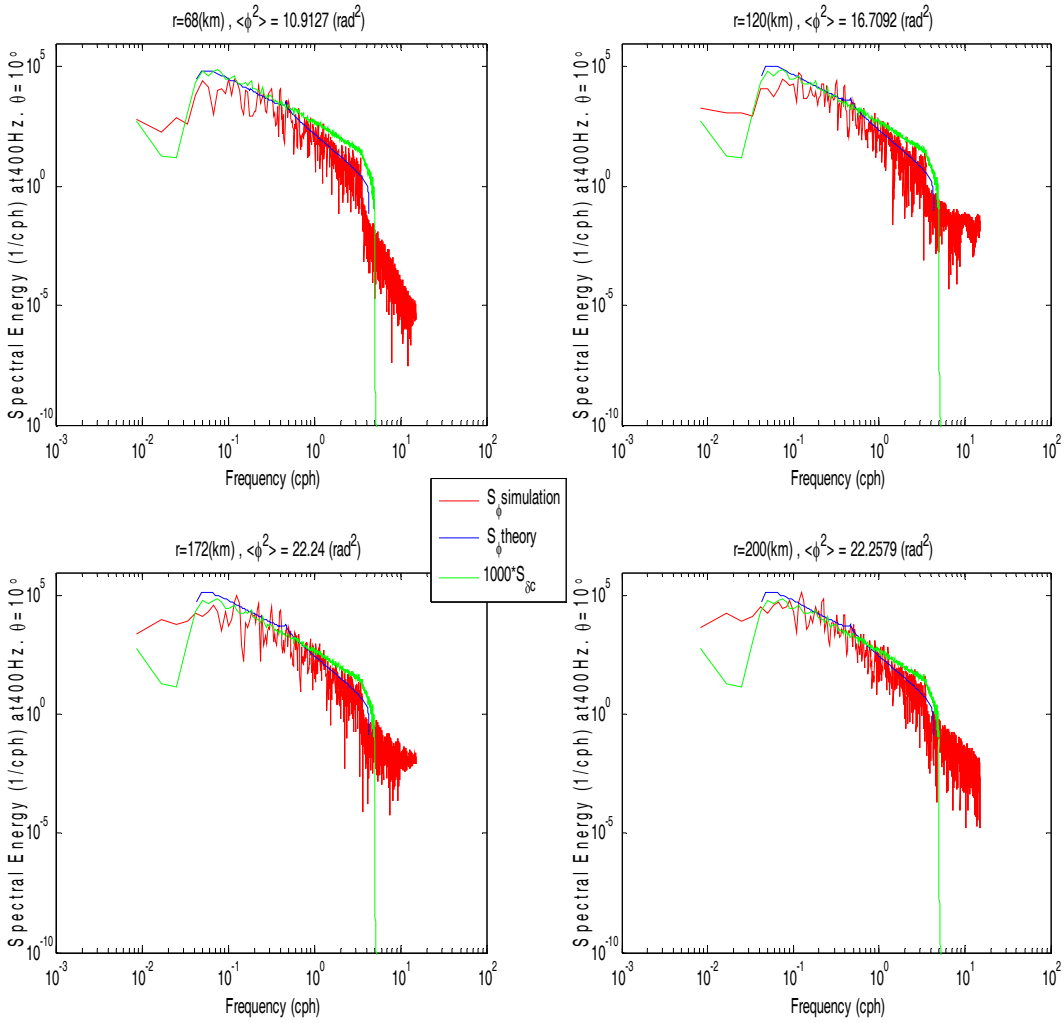

Figure 25. Phase spectra at 400 Hz and $\theta = 10°$.

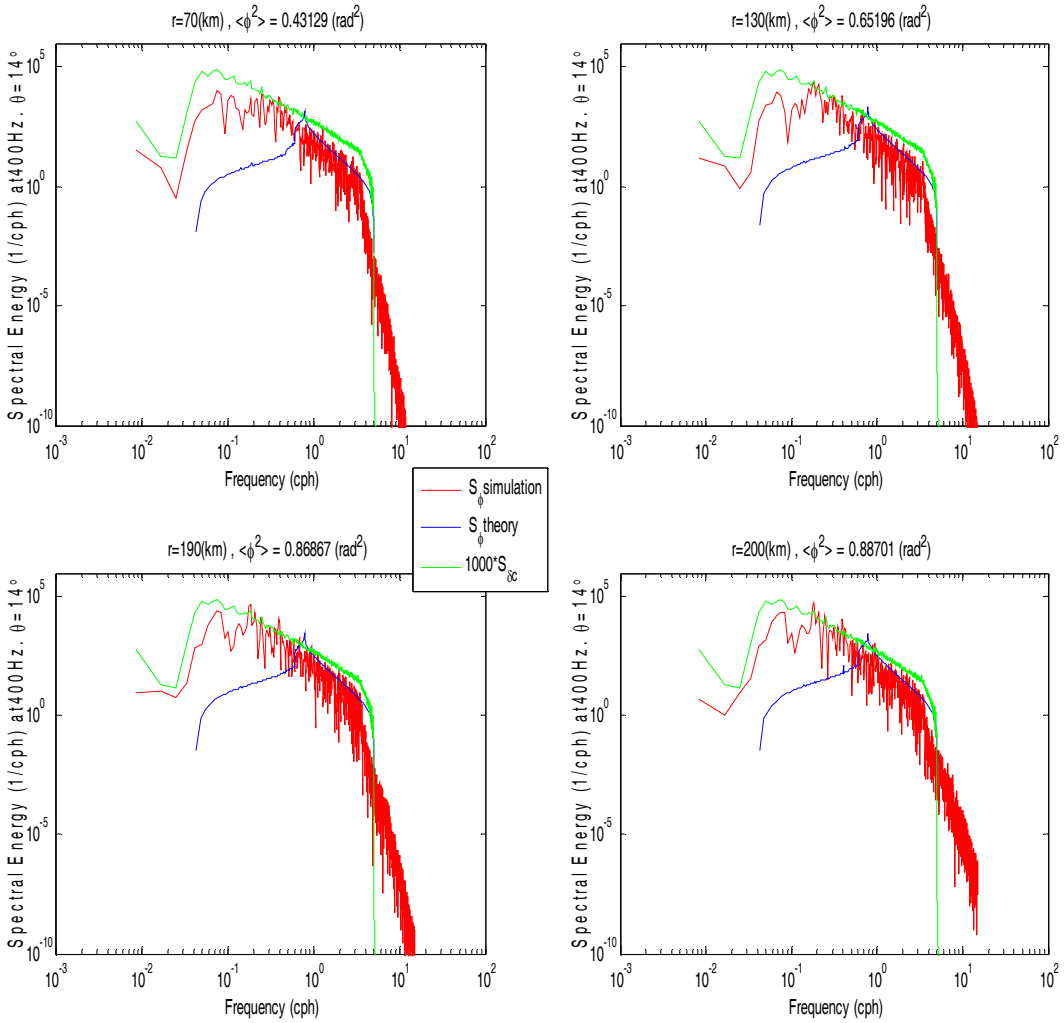

Figure 26. Phase spectra at 400 Hz and $\theta = 14°$.

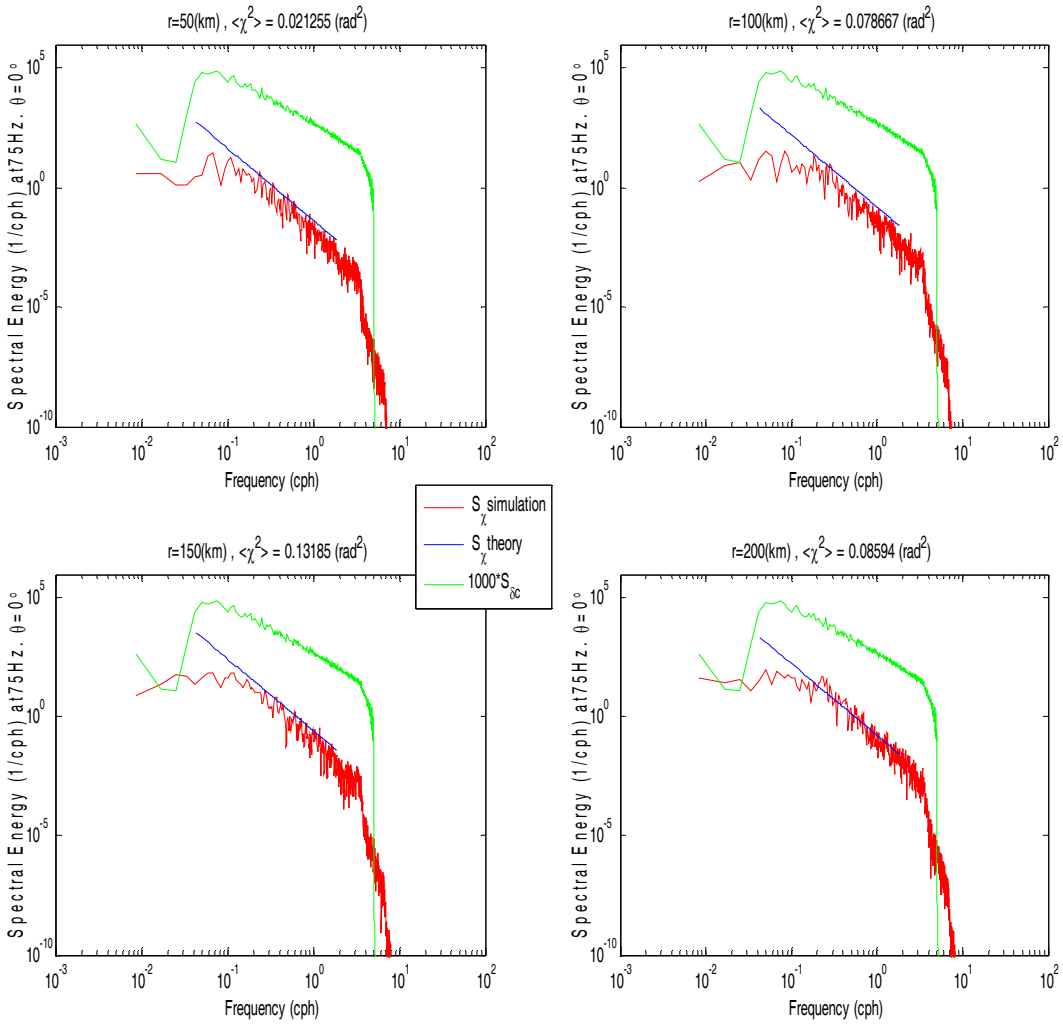

Figure 27. Log-amplitude spectra at 75 Hz and $\theta = 0°$.

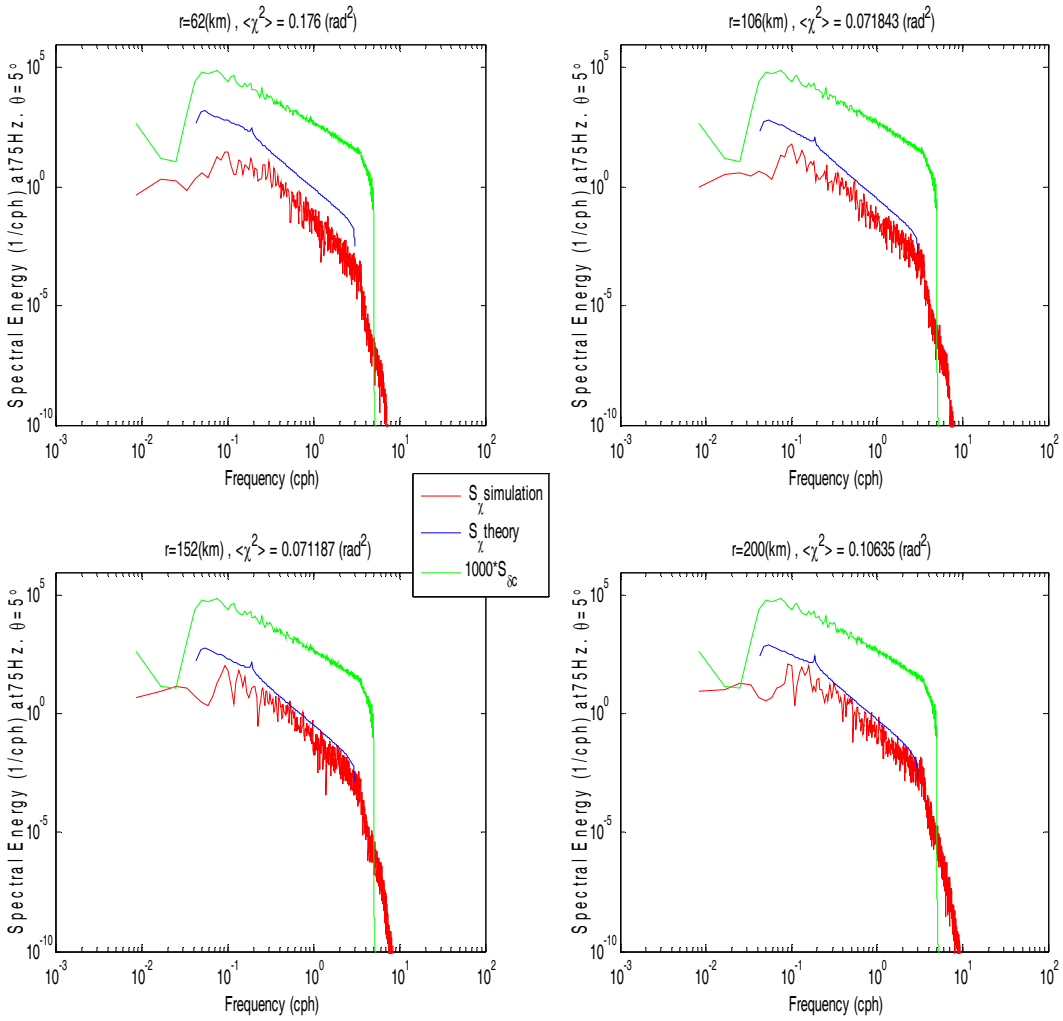

Figure 28. Log-amplitude spectra at 75 Hz and $\theta = 5°$.

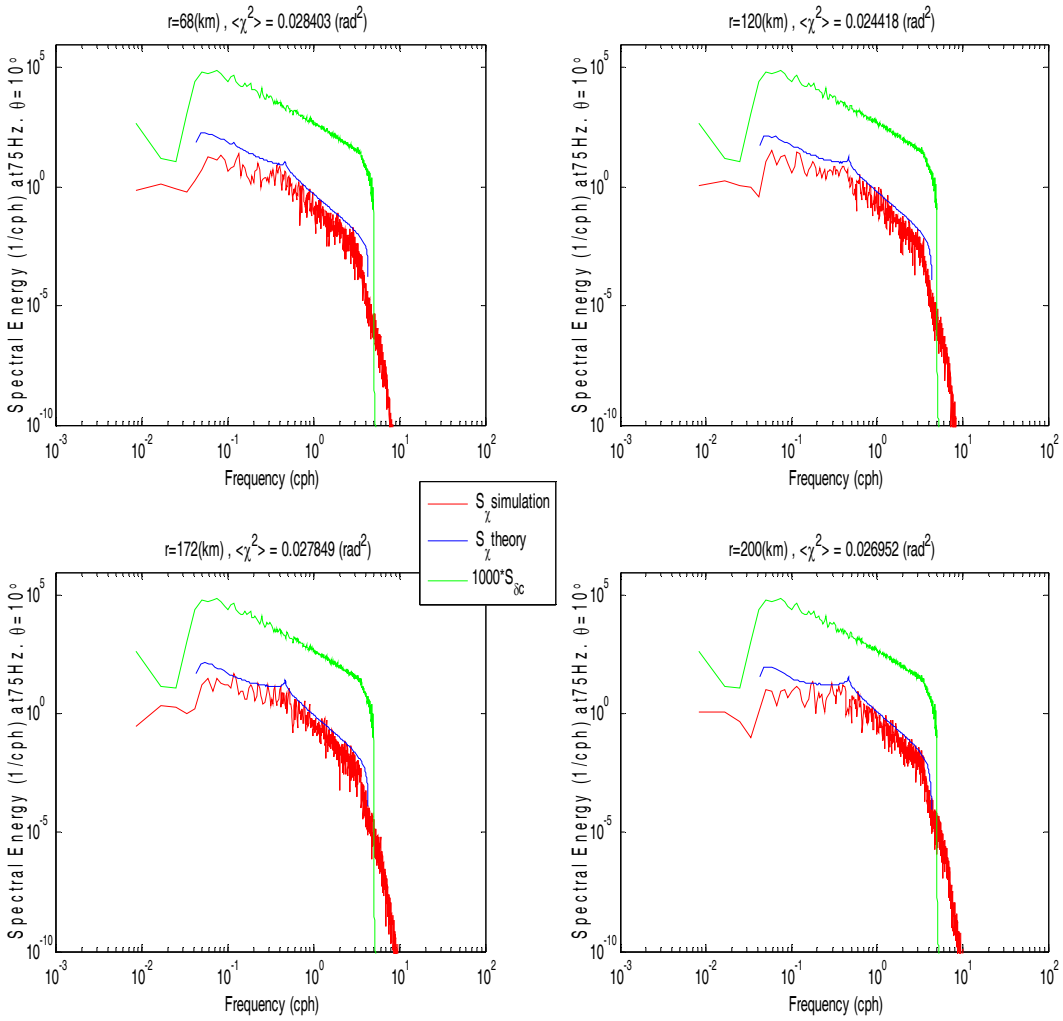

Figure 29. Log-amplitude spectra at 75 Hz and $\theta = 10°$.

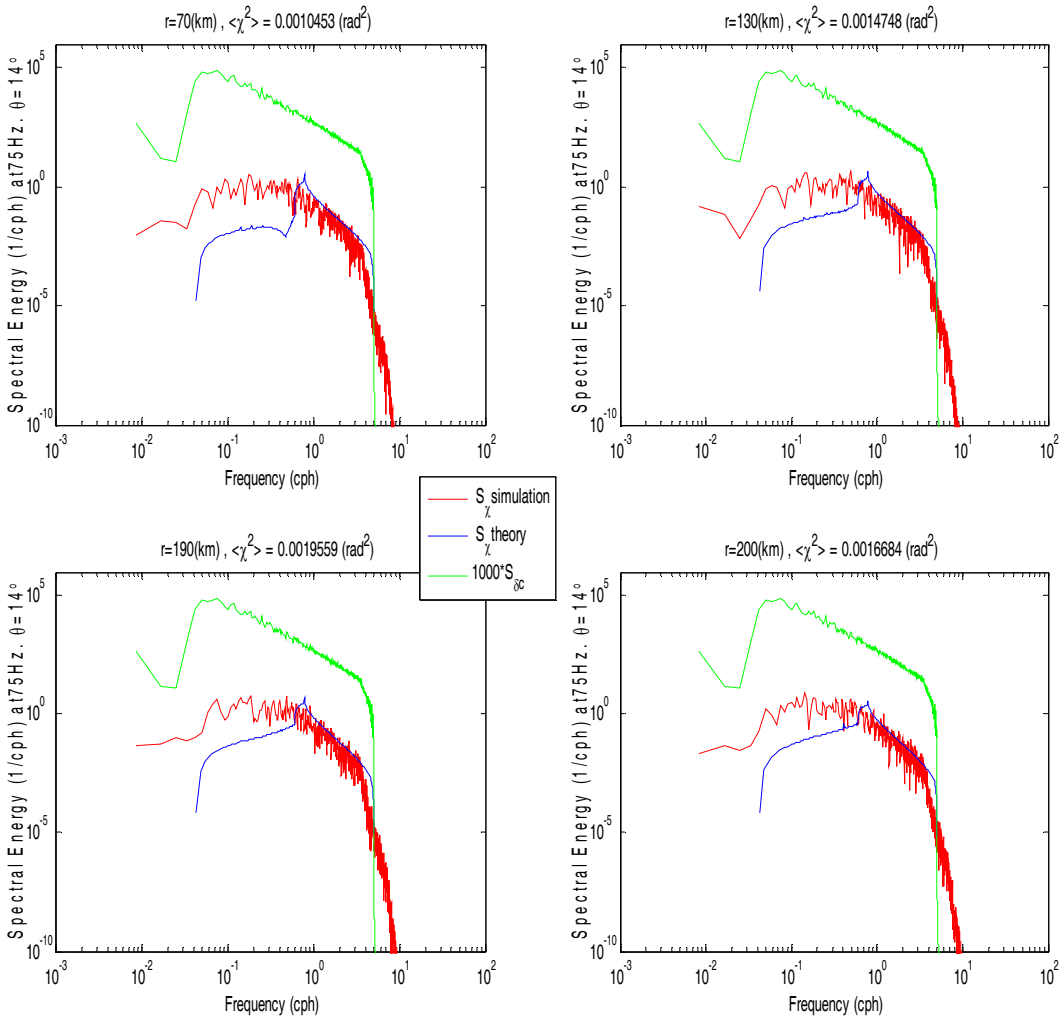

Figure 30. Log-amplitude spectra at 75 Hz and $\theta = 14°$.

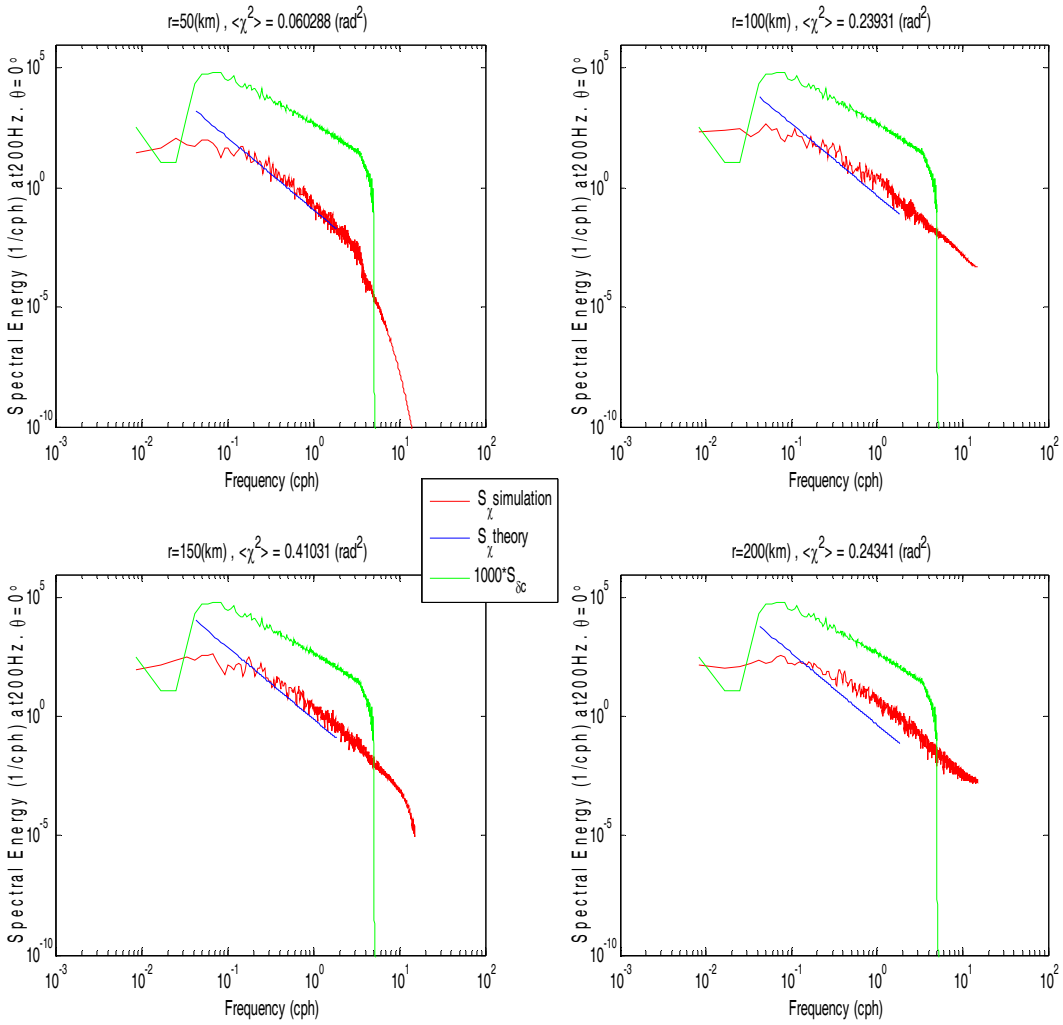

Figure 31. Log-amplitude spectra at 200 Hz and $\theta = 0°$.

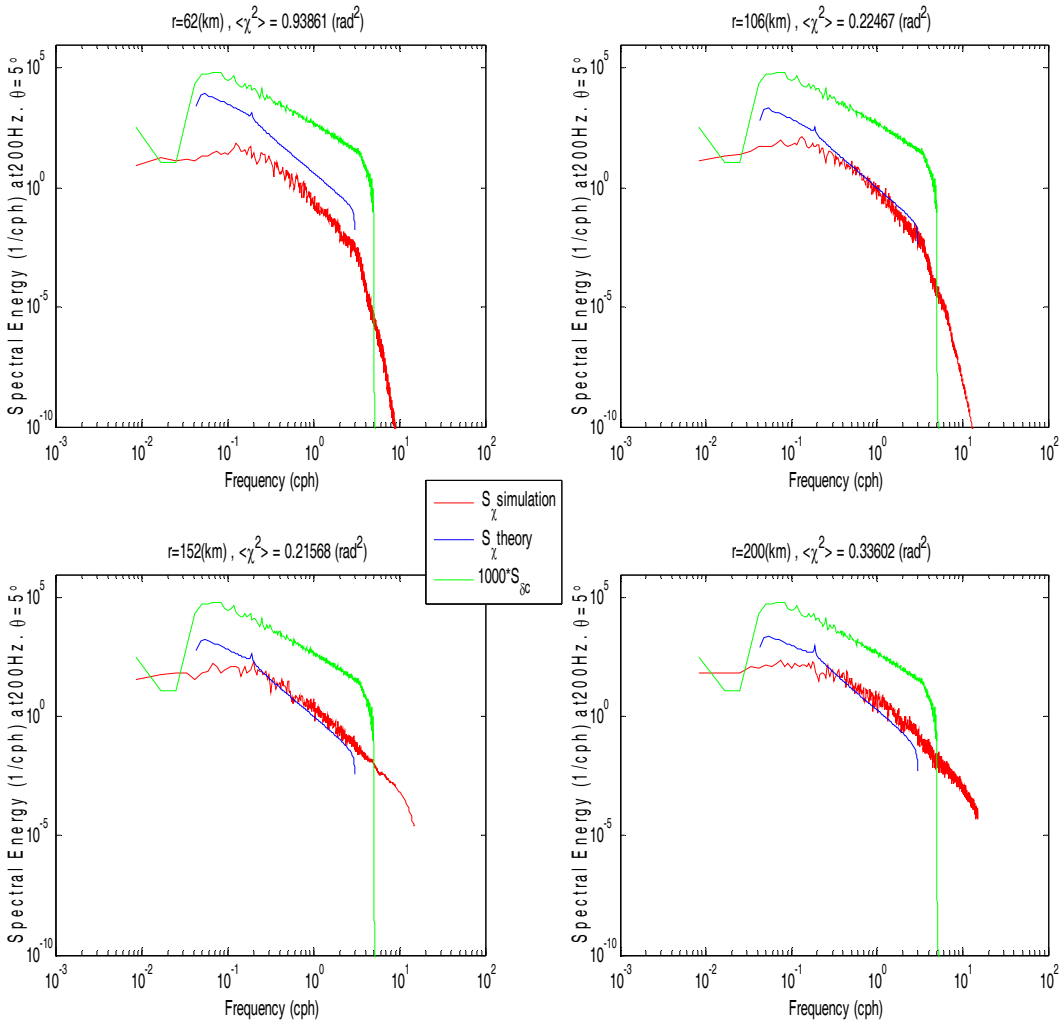

Figure 32. Log-amplitude spectra at 200 Hz and $\theta = 5°$.

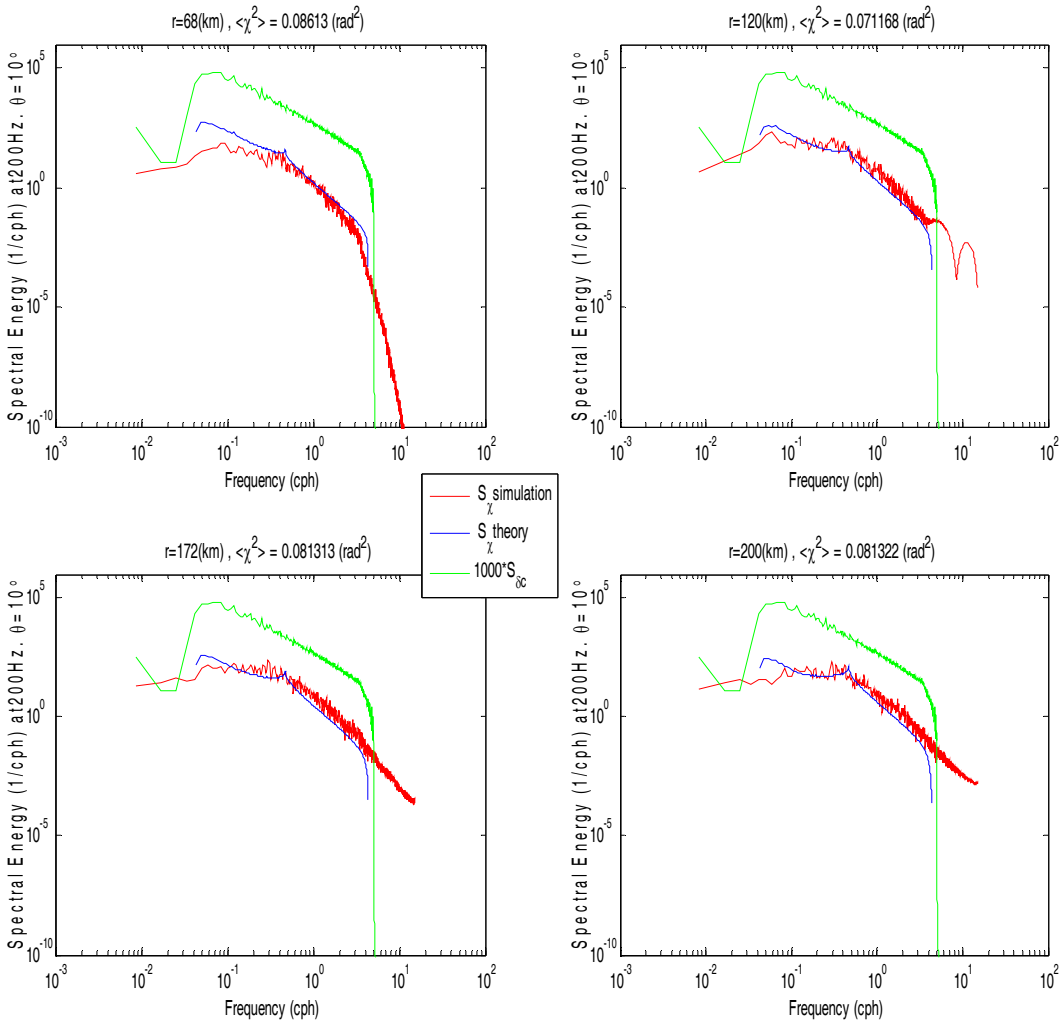

Figure 33. Log-amplitude spectra at 200 Hz and $\theta = 10°$.

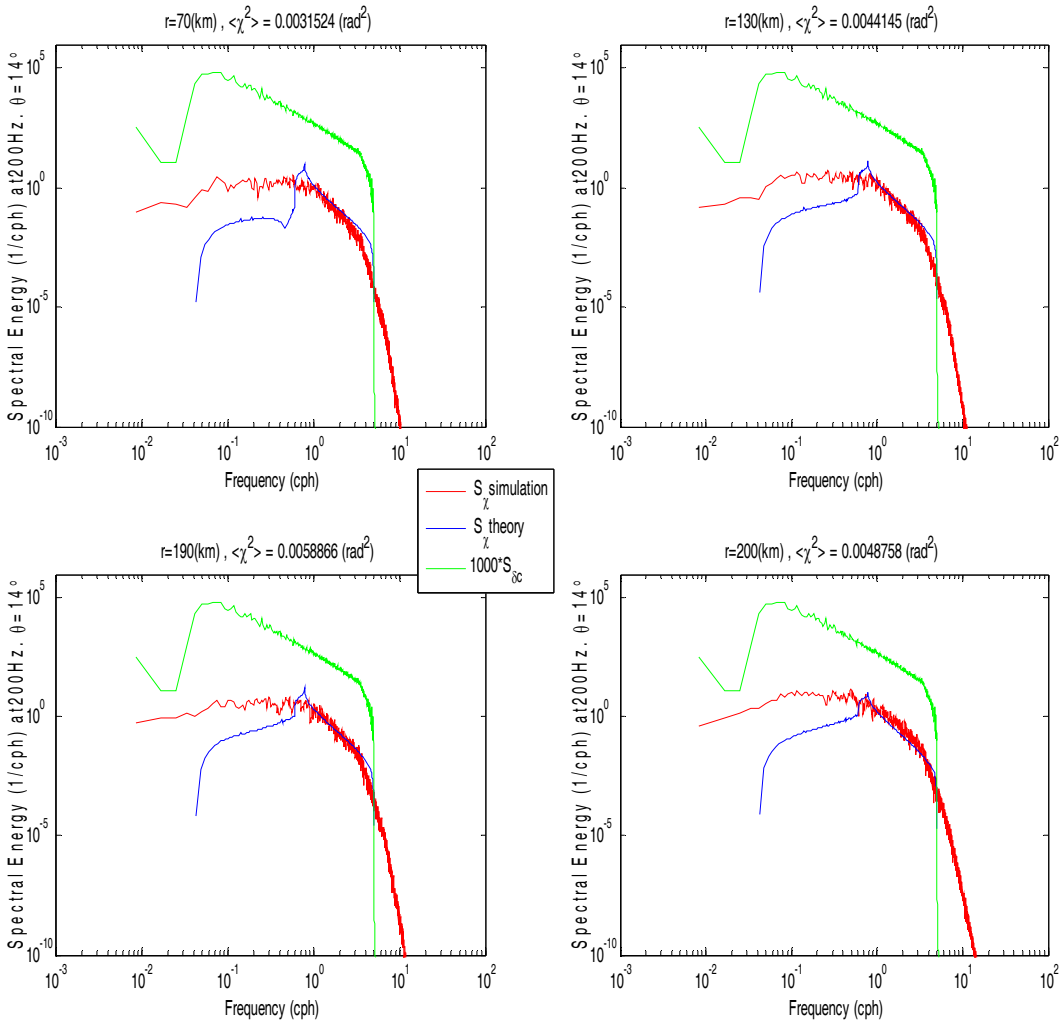

Figure 34. Log-amplitude spectra at 200 Hz and $\theta = 14°$.

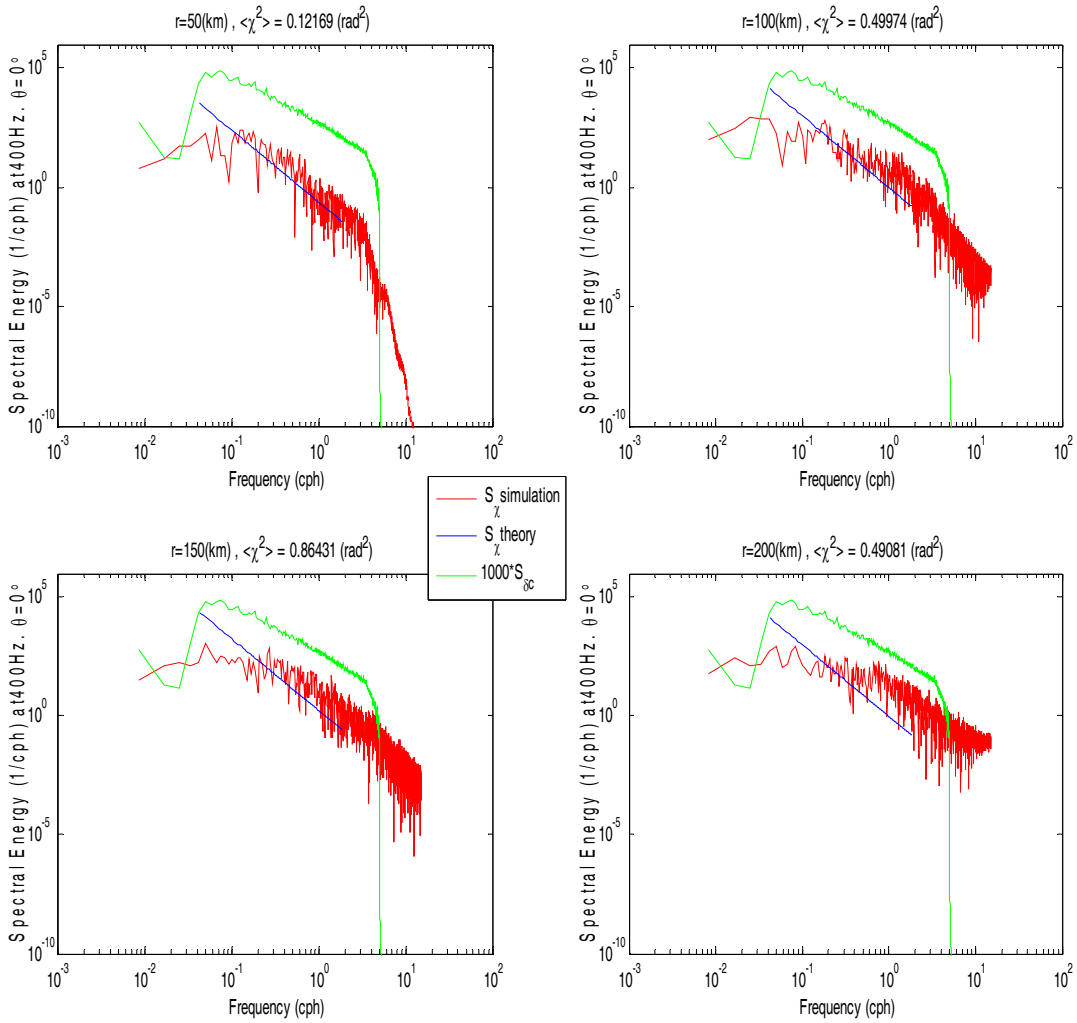

Figure 35. Log-amplitude spectra at 400 Hz and $\theta = 0°$.

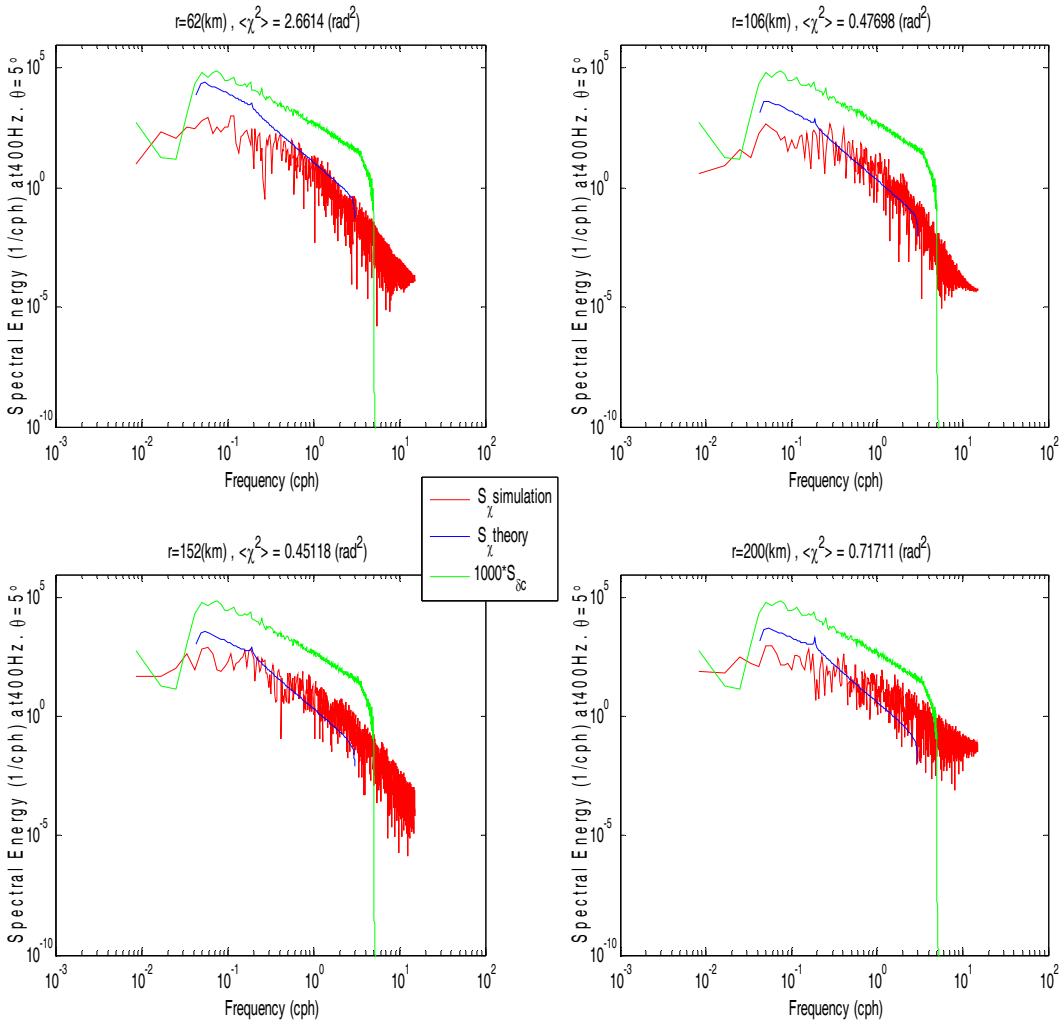

Figure 36. Log-amplitude spectra at 400 Hz and $\theta = 5°$.

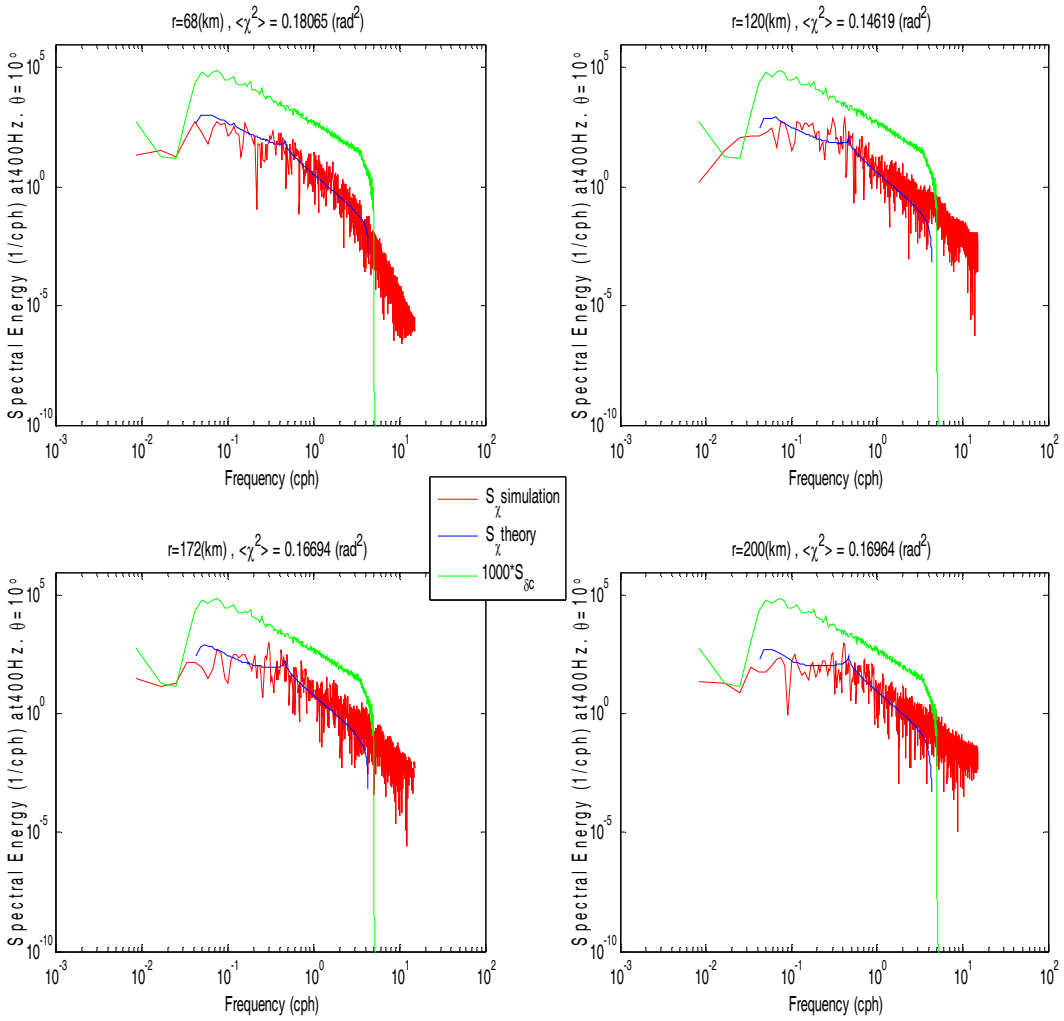

Figure 37. Log-amplitude spectra at 400 Hz and $\theta = 10°$.

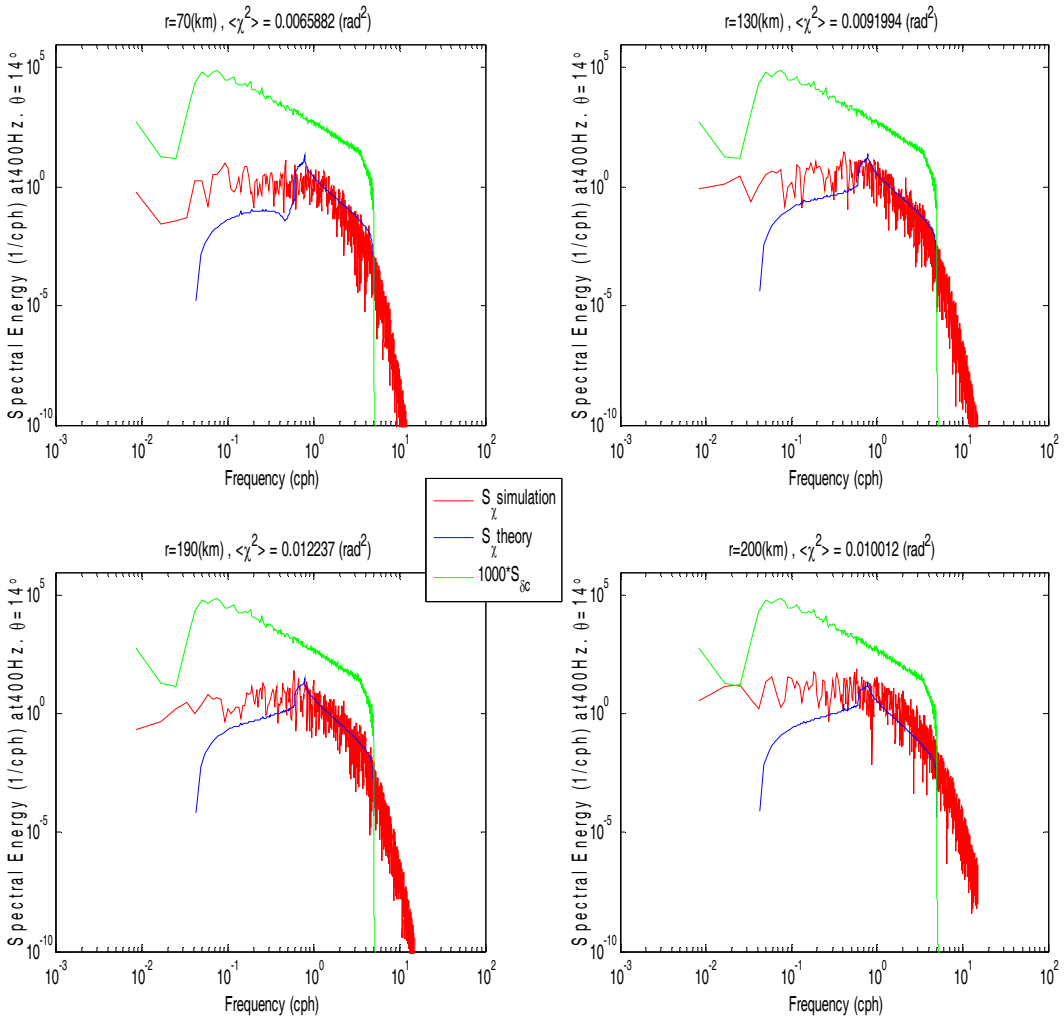

Figure 38. Log-amplitude spectra at 400 Hz and $\theta = 14°$.

LIST OF REFERENCES

Bell, J. T. Processing vertical internal-wave spectra. *J. Phys. Oceanogr.* 4: 669–670.

Colosi, J. A. 2005. WHOI/MIT 13.871 Class notes. (Unpublished).

Colosi, J. A. and M. G. Brown. 1998. Efficient numerical simulation of stochastic internal wave induced sound speed perturbation fields. *J. Acoust. Soc. Am.* 103: 2232–2235.

Colosi, J. A., J. Xu, M. Dzieciuch, P. Worchester, and B. Howe. 2007. Space-time scales of acoustic fluctuations for 75 Hz., broadband transmissions to 87 km range in the eastern North Pacific Ocean. *J. Acoust. Soc. Am.* (In preparation, Unpublished).

Duda, T. F. and C. S. Cox. 1989. Vertical wave number spectra of velocity and shear at small internal-wave scales. *J. Geophys. Res.* 94: 939–950.

Ewart, T. E. 1976. Acoustic fluctuations in the open ocean – a measurement using a fixed refracted path. *J. Acoust. Soc. Am.* 60: 46-59.

Ewart, T. E. and S. A. Reynolds. 1984. The mid-ocean acoustic transmission experiment-MATE. *J. Acoust. Soc. Am.* 75: 785-802.

Ewart, T. E., Macaskill, C., and Uscinski, B. J. 1983. Intensity fluctuations. Part II: Comparison with the Cobb experiment, *J. Acoust. Soc. Am.* 74: 1484-1499.

Ewart, T. E., S.A. Reynolds, and D. Rouseff. 1998. Determining an ocean internal wave model using acoustic log-amplitude and phase. *J. Acoust. Soc. Am.* 104: 146-155.

Flatte´, S. M. 1983. Wave propagation through random media: Contributions from ocean acoustics. *J. Acoust. Soc. Am.* 71 (11): 1267-1294.

Flatte´, S. M., R. Dashen, W. Munk, K. Watson, and F. Zachariasen. 1979. *Sound transmission through a fluctuating ocean.* Cambridge: Cambridge Univ. Press.

Garrett, C. and W. Munk. 1972. Space-time scales of ocean internal waves. *Geophys. Fluid Dyn.* 2: 225–264.

Henyey, F. and T. Ewart. 2006. Validity of the Markov approximation in ocean acoustics. *J. Acoust. Soc. Am*. 119 (1): 220-231.

Kinsler, L. E., A. R. Frey, A. B. Coppens, and J. V. Sanders. 1982. *Fundamentals of acoustics.* New York: John Wiley & Sons.

Munk, W. 1981. Internal waves and small-scale processes. *The Evolution of Physical Oceanography* edited by C. Wunsch and B. Warren. Cambridge: MIT. 264–291.

Munk, W. H. and F. Zachariasen. 1976. Sound propagation through a fluctuating stratified ocean: Theory and observation. *J. Acoust. Soc. Am.* 59: 818–838.

Pinkel, R. 1984. Doppler sonar observations of internal waves: The wave number-frequency spectrum. *J. Phys. Oceanogr.* 14: 1249–1270.

Tappert, F. D., and Hardin, R. H. 1973. A Synopsis of the AED work-shop on acoustic modeling by non-ray tracing techniques. *AESD Tech. Note TN* 73-05.

INITIAL DISTRIBUTION LIST

1. Defense Technical Information Center
   Ft. Belvoir, Virginia

2. Dudley Knox Library
   Naval Postgraduate School
   Monterey, California

3. Professor John Colosi
   Naval Postgraduate School
   Monterey, California

4. Professor Roberto Cristi
   Naval Postgraduate School
   Monterey, California

5. Professor Daphne Kapolka
   Naval Postgraduate School
   Monterey, California

6. Professor Kevin B. Smith
   Naval Postgraduate School
   Monterey, California

7. Professor Donald Brutzman
   Naval Postgraduate School
   Monterey, California

8. Professor Jeffrey Knorr
   Naval Postgraduate School
   Monterey, California

8. ARMERKOM
   Turkish Naval Research Center Command
   Pendik, Istanbul, Turkiye

9. Turkish Naval Academy
   Tuzla, Istanbul, Turkiye